Fluid Flow Modeling in Fractures

Sudipta Sarkar, M. Nafi Toksöz, and Daniel R. Burns
Earth Resources Laboratory
Dept. of Earth, Atmospheric and Planetary Sciences
Massachusetts Institute of Technology
Cambridge, MA 02139

Abstract

In this paper we study fluid flow in fractures using numerical simulation and address the challenging issue of hydraulic property characterization in fractures. The methodology is based on Computational Fluid Dynamics, using a finite-volume based discretization scheme. Steady-state, viscous, laminar flow simulations for a Newtonian fluid are carried out in both 2D and 3D fracture models. In 2D, flow is analyzed in single fractures, series and parallel combination of fractures, inclined fractures, intersecting fractures, mixed networks, and in real (rough-surface) fractures. In 3D, flow is simulated in both uniform and variable aperture fracture models. To characterize each fracture model with an *equivalent hydraulic aperture*, equations are derived for all possible scenarios followed by comparison and validation with results derived from flow simulation.

Based on the fracture models analyzed, the following are some of the important findings: 1) For fractures connected in series, the *equivalent hydraulic aperture* is a weighted harmonic mean of cubed apertures of all fractures. 2) For fractures connected in parallel, the *equivalent flow* is simply the sum of all flows through individual fractures. 3) If a fracture is inclined with respect to the axis of pressure gradient, then the amount of flow will be reduced by a factor of *cosine* of the inclination angle. 4) Any network of randomly intersecting fractures can be replaced by a single fracture to give flow equivalence; the aperture of that equivalent fracture will roughly be close to the aperture of the fracture in the network that cuts across the boundaries (inlet and outlet) in the most continuous fashion and have the smallest inclination (with respect to the pressure gradient axis). 5) For hydraulic characterization purposes, fluid flow in fractures can be sufficiently modeled using both *Stokes* and *Navier-Stokes* equations for flow *Reynolds number* upto approximately 100.

1.   Introduction

In the crust, fractures occur at various scales; they are important in hydrogeology, engineering geology, and in petroleum engineering. Fractures can act as hydraulic conductors, providing easy pathways for fluid flow, or barriers that prevent flow across them. From a geologist's perspective, a fractured reservoir is a reservoir with structural discontinuities resulting from a given paleostress history, while for a reservoir engineer it is a structural discontinuity affecting flow. Most hydrothermal-geothermal systems are found in fractured rock masses. Fractures play important role in water aquifers too. A recent estimate suggests that fractures are important in about 60% of the world's hydrocarbon reservoirs, although 'fracture denial' is not an uncommon phenomenon through the oil industry. Geologists and engineers alike are increasingly faced with evaluating the role of fractures to underpin development decisions. Fractures present both problems and opportunities for exploration and production from petroleum reservoirs. In most cases the fractures are usually important because of *permeability* rather than *porosity*. Matrix porosity stores the hydrocarbons, and fractures provide permeable pathways for the transport of hydrocarbons to producing wells.

For this research, we carried out steady-state flow simulation of a single-phase fluid using Computational Fluid Dynamics in various fractures and fracture-like idealized geometries to show how some of the fracture parameters influence fluid flow in them, and we also present quantitative analysis of fracture hydraulic conductivity and its sensitivity to some key fracture parameters.

One area of application of fluid flow modeling in fractures is the reservoir simulation of fractured petroleum reservoirs. The unexpected production behavior of many fields arising from an insufficient consideration of fracture effects on flow emphasized the need for better characterizing the fractures at various scales and transferring the meaningful part of this information to field simulation models. Nowadays, a study of fractured reservoir, from detection to full field simulation, often consists of a multi-disciplinary, integrated workflow

(Bourbiaux *et al.* 2001). The steps of such a workflow typically are: (I) Constrained modeling of the geological fracture network (Cacas *et al.* 2001), (II) Characterizing he hydrodynamic properties of the network (Sarda *et al.* 2002), (III) Choosing an appropriate flow simulation model (Jourde *et al.* 2002; He *et al.* 2001; Henn *et al.* 2000; Dershowitz *et al.* 2000; Lough *et al.* 1997; Koudine *et al.* 1998; Sarda *et al*. 1997), and (IV) Simulating reservoir flow behavior (Thomas *et al*. 1983; van Golf-Racht, 1982).

For reservoir simulation, equivalent flow properties are assigned to each reservoir cell. The determination of such effective or equivalent parameters is the most important task for simulating reservoir flow and predicting future performance yet it still is one of the most challenging tasks for the fractured reservoir simulation. For example, in a *dual porosity* or a *dual porosity-dual permeability* simulation model (Barenblatt *et al.* 1960; Warren and Root, 1963; Kazemi *et al.* 1976; van Golf-Racht, 1982; Adler and Thovert, 1999; Wu and Pruess, 2000; Consentino *et al*. 2001), an equivalent fracture permeability (or *transmissivity*) tensor is assigned to each reservoir grid cell. These estimates are used in the beginning of a simulation. In the continual process of reservoir simulation these initial estimates are perturbed and updated to match the production data as new data become available (a procedure called *history matching*). The purpose is to have a "good" reservoir model at a given time that matches the historical reservoir performance to a level that is acceptable for making reliable future forecasts. However, like any data-fitting process the final *history-matched* reservoir model is not necessarily unique! In other words, a family of permeability models may provide equally acceptable matches to past reservoir performance but may yield significantly different future predictions. To help reduce the uncertainty associated with fracture flow models, there is a need for improving the fundamental understanding of the physics of fluid flow in the complex reservoirs. In this study, we aim to enhance our understanding of the actual physics of fluid flow in fractures using Computational Fluid Dynamics methods (Chung 2002). In the following sections we will discuss the flow simulation methodology and give details of simulation results obtained for different fracture geometries.

2.   Methodology

We use numerical solution of fluid flow equations to model flow in fractures. The basic physics of fluid flow can be described by the equations of mass and momentum conservation. The equations of motion for a single-phase, Newtonian, and incompressible (constant density) fluid can be written (in scalar form) as following:-

$$\frac{\partial u}{\partial x} + \frac{\partial v}{\partial y} + \frac{\partial w}{\partial z} = 0 \qquad (1)$$

$$\rho\left(\frac{\partial u}{\partial t} + u\frac{\partial u}{\partial x} + v\frac{\partial u}{\partial y} + w\frac{\partial u}{\partial z}\right) = -\frac{\partial P}{\partial x} + \mu\left(\frac{\partial^2 u}{\partial x^2} + \frac{\partial^2 u}{\partial y^2} + \frac{\partial^2 u}{\partial z^2}\right) \quad (2a)$$

$$\rho\left(\frac{\partial v}{\partial t} + u\frac{\partial v}{\partial x} + v\frac{\partial v}{\partial y} + w\frac{\partial v}{\partial z}\right) = -\frac{\partial P}{\partial y} + \mu\left(\frac{\partial^2 v}{\partial x^2} + \frac{\partial^2 v}{\partial y^2} + \frac{\partial^2 v}{\partial z^2}\right) \quad (2b)$$

$$\rho\left(\frac{\partial w}{\partial t} + u\frac{\partial w}{\partial x} + v\frac{\partial w}{\partial y} + w\frac{\partial w}{\partial z}\right) = -\frac{\partial P}{\partial z} + \mu\left(\frac{\partial^2 w}{\partial x^2} + \frac{\partial^2 w}{\partial y^2} + \frac{\partial^2 w}{\partial z^2}\right) \quad (2c)$$

where, *u*, *v*, *w* are *x*, *y*, *z* components of velocity respectively. *Equation 1*, known as the *Continuity Equation*, and *Equation 2(a-c)*, known as the *Navier-Stokes Equation* completely describe the motion of an incompressible fluid in a continuum media in 3D (Wilkes, 1999). The assumption of incompressibility is acceptable for liquids (e.g. water, gas-free oil) under typical subsurface conditions. (Ertekin *et al.*, 2001). The compressibility effect is important for transient problems, since it contributes to the storativity of the rock/fluid system (de Marsily, 1986). However, since the relationship between fracture geometry and our key parameter of interest, *hydraulic conductivity*, is most readily studied using steady-state flow, we will ignore transient effects, and assume that the fluid density is constant. The relevant boundary conditions for the *Navier-Stokes* equations include the 'no-slip' conditions, which specify that at any boundary between the fluid and a solid, the velocity vector of the fluid must be equal to that of the solid (Paterson, 1983). This implies that at the fracture walls, not only the normal component of the velocity equals to zero, but the tangential component vanishes as well. At fluid inlet(s) and outlet(s), pressure and/or velocity boundary conditions may be specified (Paterson, 1983).

In this study, we are primarily interested in characterizing the *hydraulic conductivity* of a fractured medium, which leads to characterizing fracture *permeability*.[1] Fracture permeability is generally defined under the assumption of steady-state flow under a uniform macroscopic pressure gradient (van Golf-Racht, 1982). We will model fluid flow using the steady-state form of the *Navier-Stokes* equation, which in vector form, can be expressed as:

$$\rho\left(\mathbf{u} \bullet \nabla\right)\mathbf{u} = -\nabla P + \mu\nabla^2\mathbf{u} \qquad\qquad (3)$$

The equation is a nonlinear partial differential equation with no general solution. Generally, in order to solve it analytically, a number of assumptions will have to be made (Brodkey, 1967). The assumption of an incompressible fluid or steady-state condition is not enough to allow a general solution, because the equation is still nonlinear. One major problem in solving *Equation (3)* is the presence of the advective term, $\left(\mathbf{u} \bullet \nabla\right)\mathbf{u}$. In certain cases while modeling subsurface flow, this term is either very small, in which case it can be neglected, or vanishes altogether (Sherman, 1990). When the advective terms of the *Navier-Stokes* equation drop out, a much simpler form is obtained, which can be solved easily (Curie, 2003). Very slow (laminar), viscous flow is an example to that, and to model that fluid motion, mathematically linear *Stokes* equations can be used (Fox and McDonald, 1998; Sherman, 1990):

$$\nabla P = \mu\nabla^2\mathbf{u} \qquad\qquad (4)$$

Equation (4) can also be used to simulate flow in fractures. It is valid when the fracture walls are parallel, and is a good approximation for very low speed flows even when the fracture walls are not completely parallel. At low speeds, the effects of non-linearity – in other words the importance of advective terms – are mostly felt when there are sharp corners or bends in the fracture geometry, or when the flow is analyzed at a very fine scale near the fracture walls that have high-frequency roughness. However, from our fundamental flow simulation work in fractures we have seen that these effects do not perturb the mostly laminar and developed flow pattern that exists elsewhere in the flow path. Although eddies that are characteristics of turbulent flow can be seen near those surface irregularities, their effect on the entire flow can be evaluated by comparing results from *Stokes* solution with those of *Navier-Stokes*.

For numerical solution of steady-state *Navier-Stokes* equation, we use a commercial implementation of Computational Fluid Dynamics (CFD) techniques, named FLUENT[2]. The code uses a *finite volume* based technique to convert the governing mathematical equations to algebraic equations that can be solved numerically (Versteeg and Malalasekera, 1995). Further details about the discretization of the flow variables and different solution schemes used by the code can be found in the FLUENT documentation and also in the literature (e.g. Patankar, 1980; Issa, 1986; Berth and Jespersen, 1989; Holmes and Connell, 1989). The code is supplemented by a proprietary CAD based geometry construction and meshing engine, which allows users to build and mesh complex flow models to be used by the solver. Various features of this package makes it a more sophisticated tool than our in-house developed code.

3.   Numerical Flow Simulation

3.1 Parallel Plate Model

The simplest model of flow through a rock fracture is the parallel plate model (Huitt, 1955; Snow, 1965). This is the only fracture model for which an exact calculation of the hydraulic conductivity is possible; this calculation yields the well-known 'cubic law' (Witherspoon *et al.*, 1980). The derivation of the cubic law begins by

---

[1] The term '*hydraulic conductivity*' is used to quantify the flow transmission capacity of a single continuum (e.g. fracture), while the term '*permeability*' is used to describe the average flow capacity of larger systems, such as a porous-permeable rock, or a network of fractures.

[2] http://www.fluent.com

assuming that the fracture walls can be represented by two smooth, parallel plates, separated by an aperture *h* (*Figure 1*). Flow takes place in the space between these parallel plates – from inlet to outlet as marked by the arrows – with a commonly used boundary condition: constant static pressures at inlet and outlet. The flow space remains bounded by impermeable and rigid fracture walls (*no-slip* boundary conditions) elsewhere. The fracture width is expressed as *W*, and the distance between the inlet and outlet (fracture length) is *l*. This system creates a uniform pressure gradient which lies entirely in the plane of the fracture, resulting in a unidirectional flow through the system. The flow in this case, is in the x-direction, therefore only the x-component velocity, *u*, exists (i.e. $v = 0$; $w = 0$).

The analytical solutions for pressure and velocity are (Wilkes, 1999):-

$$P(x) = P_i - \frac{x}{l}\left(P_i - P_o\right) \qquad (5)$$

$$u(z) = \frac{1}{2\mu}\left(\frac{P_i - P_o}{l}\right)z\left(h - z\right) \qquad (6)$$

It is worth mentioning that Stokes equation (*Equation 4*) also yields the same solutions. The velocity profile, as given by *Equation (6)*, is parabolic (*Figure 2*).

The total volumetric flux through the fracture, for a width *W*, is found by integrating the velocity across the fracture from $z = 0$ to $z = h$, resulting in:

$$Q_x = -\frac{Wh^3}{12\mu}\left(\frac{P_o - P_i}{l}\right) \qquad (7)$$

The average velocity is found by dividing the flux by the cross-sectional area, *Wh*:

$$\bar{u} = \frac{Q_x}{Wh} = -\frac{h^2}{12\mu}\left(\frac{P_o - P_i}{l}\right) \qquad (8)$$

Darcy's law for flow through porous media, in one dimension, can be written as:

$$Q = -\frac{kA}{\mu}\left(\frac{P_o - P_i}{l}\right) \qquad (9)$$

The cross-sectional area *A* is equal to *Wh*. From *Equations (7)* and *(9)*, the permeability of the fracture can be identified as:

$$k = \frac{h^2}{12} \qquad (10)$$

The product of the permeability and area, also known as *transmissivity*, is equal to:

$$T \equiv kA = \frac{Wh^3}{12} \qquad (11)$$

The dependence of *T* on h^3 is the essence of the well-known cubic law.

Although exact solutions for steady-state pressure and velocity distributions are easily found for parallel plate type flow models, yet we begin by numerical solutions of flow equations for the same fracture model. This facilitates us with necessary validation of the Computational Fluid Dynamics code by checking its results against analytical (true) solutions.

4

The fracture geometry is defined by its aperture h and length l. We begin our study with 2D modeling, therefore $W = 1$ is assumed. Some 3D cases will be discussed later. In the parallel plate model, the rigid walls (fracture surfaces) are smooth and plain and have no rugosity. In steady-state conditions, the inlet and outlets are held at constant pressures, and a fully-developed flow occurs through the system. *Figure (3)* shows the results (velocity and pressure distribution) from numerical simulation in a parallel plate model. The velocity profile as seen is parabolic, with maximum value at the center, which conforms to the theory. Maximum velocity in a parallel plate model can be theoretically found by setting z = h/2 in *Equation (6)*:-

$$u_{max} = -\frac{h^2}{8\mu}\left(\frac{P_o - P_i}{l}\right) \equiv \frac{3}{2}\bar{u} \qquad (12)$$

For this and all subsequent simulations, we use an incompressible fluid with $\rho = 0.8$ g/cc, and $\mu = 5$ cp. For the model shown in *Figure (3)*, ($h = 2$ mm, $l = 80$ cm, $P_i = 200039.8$ Pa, $P_o = 200000$ Pa) there is excellent agreement between the simulation results and analytical results of the flow variables:-

	Numerical solution	Analytical solution
Mean u (m/s)	0.0033	0.0033
Mean v (m/s)	0	0
Max u (m/s)	0.005	0.005
Flow rate Q (m³/s)	6.68x10⁻⁶	6.64x10⁻⁶

The Reynold's number[3] for this problem is found as, $Re \approx 2$.

In further analysis with parallel-plate type fracture models, we investigated the effect of aperture on the volumetric flow rate through the system. For the same length l and the same inlet/outlet pressure conditions, we generated different parallel-plate fracture models by varying the aperture h, and simulated flow through each of them. It was seen that the mean velocity $\bar{u}$ varied as h^2, and the volumetric flow rate varied as h^3, as predicted by the theory.

3.2 Flow Simulation in Variable Aperture Fractures

The cubic law was derived under the assumption that the fracture consisted of a region bounded by two smooth, parallel plates. Real rock fractures, however, have rough walls and variable apertures. Furthermore, there are usually regions where the two opposing faces of the fracture wall are in contact with each other. Since transmissivity is proportional to h^3, fluid flow in a variable-aperture fracture under saturated conditions will tend to follow paths of least resistance, which is to say paths of largest aperture, and thereby depart from the rectilinear streamlines of the parallel plate model. In order to use the cubic law to predict transmissivity of a real rock fracture, one could assume that *Equation (11)* still holds if the aperture h is replaced by an equivalent aperture h_{eq}. Therefore, a more "generalized cubic law" which can be applied to any fracture geometry can be expressed as:

$$T \equiv k_f A = \frac{wh_{eq}^3}{12} \qquad (13)$$

where, k_f denotes fracture permeability. In a *dual porosity-dual permeability* reservoir simulation scheme, this k_f is used as the equivalent fracture permeability of a single simulation grid block. Therefore, if the correct h_{eq} from a distribution of fracture apertures could be determined, then a reasonable approach would be to use the following expression to characterize the equivalent fracture permeability for a reservoir simulation task:

---

[3] $Re = \frac{\rho\bar{u}L_c}{\mu}$. For internal flow in a rectangular duct, $L_c = D_h$, hydraulic diameter: 4xCross-sectional area/Wetted perimeter. For a very long and very wide channel with rectangular cross-section, $Re = \frac{\rho\bar{u} \times 2h}{\mu}$ - this is the formula that is used to compute Reynold's number for the 2D simulations in this study. Experimental evidence suggests that laminar flow may persist up to Re ~ 2300 for internal flows.

5

$$k_f = \frac{h_{eq}^2}{12} \qquad\qquad (14)$$

Computation of the correct equivalent hydraulic aperture, h_{eq}, requires solution of Navier-Stokes equations in fracture geometries that include varying aperture and obstructed regions (Zimmerman and Bodvarsson, 1996). For any fracture system, we first compute the volumetric flow rate Q [m^3/s] from our Computational Fluid Dynamics based flow simulation, and then use that to compute the equivalent hydraulic aperture of that fracture system using the following simple relation:

$$h_{eq_{simulation}} = \sqrt[3]{\frac{12 Q_{simulation} \mu l}{(P_i - P_o)}} \qquad\qquad (15)$$

3.2.1 Fracture Connected in Parallel

A *parallel combination* of n equi-length fractures implies that they all are subject to the same pressure gradient (analogous to resistors connected in parallel in electrical circuits experiencing equal amount of potential difference across them). For such a case, using the same principle of computing equivalent resistance (or conductance) of parallel resistors, a rule for computing the equivalent hydraulic aperture for fractures connected in parallel can be established as:

$$h_{eq_{parallel}} = \sqrt[3]{\sum_{i=1}^{n} h_i^3} \qquad\qquad (16)$$

The equivalent (or total) flow rate through the system will simply be the sum of flow rates through each individual fractures:

$$Q \equiv \frac{h_{eq}^3}{12\mu}\left(\frac{P_i - P_o}{l}\right) = \sum_{i=1}^{n} Q_i \qquad\qquad (17)$$

To test the validity of this rule, we do a simulation with three distinct fractures connected to parallel. While they have different apertures (2 mm, 0.5 mm and 1 mm), their lengths are same (80 cm) and are connected to the same inlet and outlet (pressure differential between inlet and outlet is 190 Pa). The pressure and velocity distribution from the simulation are plotted on *Figure 4*. The numerical solution yields a flow rate Q = 3.615x10^{-5} m^3/s, which gives h_{eq} = 2.09 mm according to *Equation (15)*. The network rule, according to *Equation (16)*, predicts h_{eq} = 2.09 mm, which is exactly equal to the result obtained from actual flow simulation. Therefore, it is verified that *Equation (16)* provides a good estimate of the equivalent fracture hydraulic aperture of a fracture network where individual members are arranged in parallel with the axis of pressure gradient.

Also revealed from this simulation is that most of the flow is through the thickest fracture. The 2 mm fracture occupies 57% of the total available flow area in the system, but it transports about 87% of the total flow. Therefore, a general conclusion for parallel networks is that, when there are fractures of different apertures in a parallel network, a single fracture that is flow equivalent to that network will have an aperture magnitude (h_{eq}) close (and slightly larger) to the aperture of the thickest fracture (*thickest = largest aperture magnitude*) of the original network.

3.2.2 Fractures Connected in Series

In a series combination of fractures, the same Q prevails through each member of the fracture network. Again, using the series connection of resistors analogy, the following formula can be used to compute the equivalent fracture aperture:

$$h_{eq_{series}} = \frac{1}{\sqrt[3]{\sum_{i=1}^{n} \frac{l_i}{l}\left(\frac{1}{h_i^3}\right)}} \qquad (18)$$

where, l_i and h_i are the length and aperture of the ith fracture section; l is the total length of the series network, i.e. distance between inlet and outlet. It is noted that the derivation of this expression is based on the assumption that each fracture section of the network has the ideal parallel plate geometry; therefore n is the total number of "parallel plate" fracture members connected in series.

To predict the equivalent hydraulic aperture by *Equation (18)*, information about the length (l_i) of individual fracture section that has uniform aperture (h_i) is required. For real complicated reservoir fractures, such a precise description of fracture geometry involving knowledge of l_i would be very restrictive, if not impossible. The longitudinal variation of apertures in real fractures will be much more high frequency, severe and consequently very difficult to determine. Therefore, it should be noted that *Equation (18)* will have limited use in characterizing equivalent fracture hydraulic aperture. It could only be applied for relatively simple geometries, or where the aperture field varies smoothly along the fracture length.

To test the validity of *Equation (18)*, a flow simulation is carried out in a series network of fractures with three distinct fracture elements having different aperture magnitudes (0.5 mm, 1 mm, and 2 mm). The equivalent aperture of the network is computed from the simulation derived flow rate (Q) using *Equation (15)*, which is then compared to the theoretically predicted equivalent aperture magnitude given by *Equation (18)*. We do this for a number of series networks, which we generate by simply varying the length fractions and topology of connection of the three fracture elements. The following table summarizes the model properties of couple of series cases and also shows the comparison between equivalent aperture values computed from numerical simulation and network formula:

	l_i cm	h_i mm	h_{eq} (mm) simulation:Eqn.15	h_{eq} (mm) theory:Eqn.18
Case a	45	2		
	15	0.5	0.822	0.819
	20	1		
Case b	15	2		
	45	0.5	0.597	0.594
	20	1		

[Case a: $\Delta P = 114.8$ Pa, $Q = 1.33 \times 10^{-6}$ m^3/s]
[Case b: $\Delta P = 300.1$ Pa, $Q = 1.33 \times 10^{-6}$ m^3/s]

While constructing each of these models, total length was kept fixed ($l = 80$ cm). Velocity distribution obtained by flow simulation for *Case a* - mainly showing regions of geometry variations - is shown by *Figure 5*. Velocity distribution for Case b (not plotted) exhibits identical characteristics. As seen from these cases, the series network formula (*Equation 18*) has good accuracy in predicting equivalent hydraulic apertures. The theoretical expression for equivalent aperture (*Equation 18*) assumes fully-developed laminar flow in each fracture section and does not take into account the non-linearity produced due to geometry change. In reality, non-linearity in flow variables do occur at the intersection of two different fracture sections; however the flows in these models are so slow that these non-linear behaviors are very localized and do not affect the flow in other parts of the model. Therefore, the effects of such geometry variation are negligible in terms of their influence on velocity distribution in the entire model, and hence we see a very good agreement between the equivalent aperture magnitudes predicted by theory and computed from simulation.

3.2.2.1 Length of fracture members in a series network unknown

From *Equation (18)*, it is seen that the equivalent hydraulic aperture of a series network is a weighted harmonic mean of the cubic apertures of participating fracture members, the weights being the length fractions (l_i / l) of respective members. In reality, however, these length fractions are difficult to get. Therefore, given only a distribution of apertures $\{h_i\}$, it is important to know the likely range of equivalent aperture magnitude the fracture network may have. For example, we take an 80 cm long fracture composed of three discrete fracture elements

7

having apertures 0.5 mm, 1 mm and 2 mm. We assume that the lengths of these individual elements are unknown. We employ a routine to compute all possible values of equivalent hydraulic apertures for different combinations of length fractions of individual members (i.e. using *Equation 18* for each realization). With 1 cm accuracy in length, there are 3081 possible combinations of length fractions and the histogram of equivalent apertures has a shape as shown by *Figure 6*. The equivalent aperture of this series network is minimum (*min = 0.5039 mm*) when the thickest fracture section is the shortest (1 cm) and the thinnest section is the longest (78 cm); and it is maximum (*max = 1.6219 mm*) when the thickest section is longest (78 cm) and the thinnest section is shortest (1 cm) (illustrated by *Figure 7)*. This, of course, is intuitive and obvious, but what is not so obvious is where the mean of equivalent apertures will be located. In this example, the *mean* is calculated as *0.7548 mm*. It is found that more than one combination results in such an equivalent aperture. These are:

l_1 , h_1	l_2 , h_2	l_3 , h_3	h_{eq}
7, 2	16, 0.5	57, 1	0.755
15, 2	17, 0.5	48, 1	0.755
23, 2	18, 0.5	49, 1	0.755
31, 2	19, 0.5	30, 1	0.755
39, 2	20, 0.5	21, 1	0.755
47, 2	21, 0.5	12, 1	0.755
55, 2	22, 0.5	3, 1	0.755

We further investigate the issue of how the range of equivalent aperture values change as we include additional fracture elements. We repeat our analysis by changing our original 3-tier aperture configuration as follows: 1) Adding a fracture section of a relatively small aperture, *0.1 mm* (this could represent a case when the void space in fractures are sealed due to chemical or other reactive process during transport), 2) Adding a fracture section of a relatively large aperture, *1.9 mm* (this could represent a case when fractures are propped open naturally due to fluid pressure or artificial stimulation such as *hydrofrac*), 3) Adding both small (*0.1 mm*) and large aperture (*1.9 mm*) fractures. The total length remains the same (80 cm) in each of the cases, and we combine the set of fractures in series in all possible ways (by varying the length fraction of individual members) and compute the equivalent fracture apertures for each different scenario. We summarize some statistics of the results in the following table:

$\{h_i\}$	Min h_{eq}	Max h_{eq}	Mean h_{eq}	Std. h_{eq}
{0.5, 1, 2}	0.504	1.622	0.755	0.179
{0.5, 1, 2, 0.1}	0.101	0.428	0.189	0.069
{0.5, 1, 2, 1.9}	0.506	1.621	0.834	0.201
{0.1, 0.5, 1, 1.9, 2}	0.102	0.428	0.204	0.073

The histogram from each of these experiments has a shape similar to that of *Figure 6*. When the lengths of individual fractures are not known, this type of analysis can provide useful bounds for equivalent hydraulic parameter estimates.

3.2.2.2 Effect of Constrictions

For practical purposes, very often fractures are modeled as media bounded by *parallel plates* with rough fracture walls represented by straight line segments (*Figure 8*). As the effect and importance of fracture *apertures* (distance between fracture walls) are widely discussed, little is known about the role of *constrictions* in fracture modeling. In this paper, we use the term 'constriction' to define the wall-to-wall distance at the plane of intersection between two fractures (*Figure 8*). In this section, we do some flow simulation to investigate the effects of constrictions on flow through fractures. We present simulation results from two cases where we have the same three fractures (2 mm, 0.5 mm, 1 mm) connected in series, but different types of connectivity.

Figure 9 plots the geometry and connectivity of one of the models and also shows some simulation results. The sequence of wall-to-wall distance (*mm*) can be written as: S1 $\equiv$ {2 0.5 0.5 0.5 1}, where the underlined numbers indicate constrictions, c_i and the rest just being the apertures, h_i. The steady-state flow solution for this

8

model yields a total flow rate, $Q = 1.33x10^{-6}$ m^3/s for a pressure differential $\Delta P = 114.9$ Pa between the inlet and outlet, which – by *Equation (15)* – gives an equivalent aperture of *0.822 mm* for this model. This is in good agreement with the simulation results of previously modeled *Case a* (*Figure 5*), which essentially had the same fracture members having same length and aperture but connected in a slightly different manner. We present another model (*Figure 10* [a]) where the sequence of wall-to-wall distance (in *mm*) is: S2 ≡ {0.5 <u>0.25</u> 2 <u>0.75</u> 1}, the underlined numbers being the constriction magnitudes, c_i. Some of the simulation results for this model are presented on *Figure 10 [b,c,d]*. The steady-state flow solution for this model yields a total flow rate, $Q = 1.33x10^{-6}$ m^3/s for a pressure differential $\Delta P = 306.6$ Pa between the inlet and outlet, which – by *Equation (15)* – gives an equivalent aperture of *0.5927 mm* for this model. The model has same {l_i, h_i} as *Case b* discussed under Section 3.2.2 (Fractures Connected in Series), but the magnitudes of constrictions are different. The slight difference in results between this one and *Case b* is due to this geometry difference at intersections. To relate the issue of constriction with fluid motion, we note that in the first model of this section (sequence S1) both constriction values are equal to at least one of their adjacent aperture values, however in the second model (sequence S2) the constrictions are not equal to any of their adjacent apertures. (We label the constrictions of sequence S1 and sequence S2 as 'smooth' and 'non-smooth' respectively). To better understand how velocity magnitudes vary at different sections of the fracture (including at intersections/constrictions), a plot of x-velocity at different constant-x surfaces for the model described by sequence S2 is given on *Figure 11*.

Due to the possibility of stark velocity contrast at 'non-smooth' constrictions at fracture intersections, we propose that the calculation of equivalent hydraulic aperture must also take into account the effect of constrictions. Therefore, we suggest the following modification to *Equation (18)*:

$$h_{eq_{series}} = \frac{1}{\sqrt[3]{\sum_{i=1}^{n} w_{hi}\left(\frac{1}{h_i^3}\right) + \sum_{i=1}^{n-1} w_{ci}\left(\frac{1}{c_i^3}\right)}} \quad (19)$$

where, w_{hi} is the weight associated with aperture h_i (it is the length fraction, l_i/l), and w_{ci} is the weight associated with constriction c_i. For most cases, $w_{ci} << w_{hi}$. In the limiting cases where constrictions are 'smooth', i.e. they are equal to one of the adjacent aperture magnitudes (for example sequence S1), w_{ci} can be treated as zero, and *Equation (19)* reduces to *Equation (18)*. However, when constrictions are 'non-smooth', i.e. their magnitudes are different than any of the adjacent aperture magnitudes (for example sequence S2), use of w_{ci} may be necessary. Work is currently under way to understand more about the effects of constrictions and connectivity of series fractures on fluid flow.

3.2.3 Combination of Series and Parallel Fractures

In this section, we present simulation results for a fracture network having a combination of series and parallel connections (*Figure 12*). Fractures *f2*, *f3*, *f4* and *f5* are connected in parallel, and their combination is connected in series with fracture *f1*. The system has only one inlet, but four different outlets. The flow solution gives a total flow rate $Q = 1.334x10^{-6}$ m³/s for $\Delta P = 116.4$ Pa, which yields an equivalent aperture of *0.8194 mm*. Using theoretical expressions for series and parallel connections (*Equations 16 & 18*) the equivalent hydraulic aperture is predicted as *0.7539 mm*. The difference is explained by the fact that the simulation takes into account all the non-linearity that are present in the real model, however the network formulae consider each fracture member as ideal parallel-plate model and the non-linearity at the intersection of fractures are not accounted for by the theoretical expressions. The flow simulation provides more accurate estimate of equivalent aperture magnitudes as it models the real physics of fluid flow rather than any idealized approximation.

Difficulty arises when the network topology is not known. In such a situation, a reasonable estimate of the equivalent hydraulic aperture could be the following:

$$h_{eq_{series}} \le h_{eq} \le h_{eq_{parallel}} \quad (20)$$

9

Inequality (20) gives an expression for the upper and lower bounds of the equivalent hydraulic aperture, h_{eq}, for any network of connected fractures. The upper bound, $h_{eq_{series}}$, is the equivalent aperture if all the participating fractures in the network were connected in series, while the lower bound $h_{eq_{parallel}}$ is again the equivalent aperture if all the participating fractures in the network were connected in parallel. In reservoir simulation, where the connectivity of fracture networks is not well known, these bounds could be used; such bounds may be useful in a stochastic simulation. For the model shown in this paper (*Figure 12*), $h_{eq_{series}}$ and $h_{eq_{parallel}}$ are computed as *2.023 mm* and *0.2906 mm* respectively, which readily verifies Inequality (20) as h_{eq} was computed as *0.7539* mm by using the network formulae.

Madden (1976) investigated random networks as models of heterogeneous media and concluded that for small contrasts, networks tend toward the geometric mean. For a combination of series and parallel fractures, this implies that the *geometric mean* of a given aperture distribution, $\{h_i\}$, could be used as an estimate for the equivalent hydraulic aperture of that network. For any set of numbers, its geometric mean (*GM*) is bounded by its arithmetic mean and (*AM*) and its harmonic mean (*HM*):

$$HM \leq GM \leq AM \qquad\qquad (21)$$

Inequalities (20) & (21) are analogous: $h_{eq_{series}}$ and $h_{eq_{parallel}}$ are indeed some variants of *HM* and *AM* of $\{h_i\}$, respectively. Therefore, when deterministic facts about the fracture network are not known, using the *GM* of $\{h_i\}$ as an estimate of h_{eq} is justified. However, the accuracy of this estimate will vary from one model to another, and is subject to further analysis. For example, the GM of apertures of the model shown by *Figure (12)* is *0.464 mm*, while its theoretically predicted h_{eq} = *0.754 mm* – resulting in an error of about 38% if *geometric mean* is used.

We also investigate what percentage amount of total flow is carried to the outlet by each fracture leg connected in parallel for this network model. Theoretically, volumetric flow rate varies as h^3 (*Equation 7*), and therefore the thicker fractures will always be dominating in the vicinity of thinner fractures. For example, fracture *f5* constitutes only 42% opening of the total available fracture area to the outlet, yet it carries 77% of the total flow to the outlet. This has important implications in oil production, because the majority of the flow towards the well from a complex fractured reservoir will be through larger aperture fractures and only those can be targeted to boost production.

3.3 Inclined Fractures

In this section, we study flow through inclined fractures – fractures that are oriented at angle with respect to the overall (macroscopic) pressure gradient axis that controls flow, as shown by *Figure 13*.

Figure 14 shows the results of a flow simulation in a fracture model, which is embedded in a rock slab that is subjected to a horizontal pressure gradient. The surface of the fracture forms a 45° angle with the axis of pressure gradient. From visualization of the results, it becomes clear that the actual physics of flow requires the equi-pressure lines (shown by pressure contours in *Figure 14 (a & b)*) inside the fracture to have an orientation normal to the fracture walls/surfaces[4]; and as a consequence, the flow, which should be normal to the tangents drawn on equi-pressure surfaces, is aligned with the fracture orientation. The same physics should hold for all laminar flows in any orientation of a fracture. To validate this, we ran simulations in single fractures oriented at some other angles: 20°, 30°, and 70°, and found that the average direction of the velocity vectors were 20°, 30°, and 70°, respectively. Likewise, if there are multiple oriented fractures with different orientations inside a rock slab, in each of those fractures the flow will perfectly align with its channel direction and so will the pressure gradient axis, regardless of the macroscopic pressure gradient direction that exists due to the boundary conditions (inlet and outlet)

---

[4] Except for very close to the inlet and the outlet. The pressure anomaly near those boundaries is a consequence of the fluid entering and leaving the system (rock) horizontally. We also studied flow by forcing the fluid to enter and leave at 45°, and found that the overall difference in flow between the two cases is negligible.

of the rock. This is an important understanding that forms the rationale to justify an equation to calculate flow rate and effective permeability for oriented fractures, which we will present shortly.

3.3.1 Numerical Experiment

To find an expression for computing steady-state flow rate in oriented fractures, we did a numerical experiment. We took a simple parallel plate fracture model having an aperture (h) of 1 mm, and oriented it at different angles inside our rock slab model (as *Figure 13*). Holding the pressures at inlet and outlet constant, we ran flow simulations in each of those oriented fracture models. Each flow simulation yields a steady-state volumetric flow rate Q. The following is a summary of this numerical experiment:

True fracture aperture h [mm]	Fracture orientation θ [degree]	ΔP (=P1-P2) [Pa]	Length of the rock slab l [cm]	Q (10^{-6} m³/s)
1	0	123	20	10.25
1	20	123	20	9.63
1	30	123	20	8.87
1	30	61.6	20	4.45
1	45	123	20	7.24
1	70	123	20	3.49

Analyzing these data, empirically we find the following expression that relates the flow rate to its function parameters:

$$Q = \frac{h^3 \cos\theta}{12\mu}\left(\frac{\Delta P}{l}\right) \qquad (22)$$

Comparing *Equation (22)* with *Darcy's Equation*, the magnitude of permeability in the direction of macroscopic pressure gradient can be expressed as:

$$K = \frac{h^2}{12}\left(\cos\theta\right) \qquad (23)$$

The essence of Equation (22) is that the flow rate is decreased by a factor of $\cos\theta$ due to inclination (where $-\pi/2 \le \theta \le \pi/2$). Similarly, permeability is reduced by the same factor as shown by *Equation 23*. A physical explanation to this is the effect of added length of fracture (the actual length of the fracture is increased by $\frac{l}{\cos\theta}$). As explained earlier, inside the inclined fracture the pressure gradient and the velocity have same direction; therefore the only thing that makes a difference in the inclined fracture case as compared to the horizontal fracture case is just that added length, hence $\cos\theta$.[5]

---

[5] We note a significant disagreement between our analysis and what currently exists in the major literature. Originally proposed by Parsons (1966), and thereafter adopted in standard reservoir engineering literature (e.g. van Golf-Racht 1982, Nelson 2001, etc.) the discriminating factor is $\cos^2\theta$, as opposed to our proposed $\cos\theta$. The present-day literature states: $Q = \frac{h^3 \cos^2\theta}{12\mu}\left(\frac{\Delta P}{l}\right)$, and $K = \frac{h^2}{12}\left(\cos^2\theta\right)$, which may cause significant difference in estimation of these important properties, when there are large number of oriented fractures. We could not find numerical verification of these equations with *Navier-Stokes* flow simulation. While further investigation may be required to completely resolve this discrepancy, our formulation, which is backed by numerical analysis and visualization of the true physical behavior, seems much more insightful and reliable at this point.

3.3.2 Equivalent Hydraulic Aperture

The concept of equivalent hydraulic aperture (h_{eq}) can be applied in oriented fractures as well, and we use the values reported on the previous table to calculate h_{eq} for each model using *Equation (15)* :-

θ [degree]	True h [mm]	h_{eq} [mm]
0	1	1
20	1	0.98
30	1	0.95
45	1	0.89
70	1	0.70

The effect of fracture inclination in the hydraulic conductivity is also illustrated graphically (*Figure 15*).

3.3.3 Effect of Fracture Orientation in a Series Network

Applying *Equation (22)* in a series network, we derive the following expression for calculating the *equivalent hydraulic aperture* of a system which is composed of *n* fracture members connected in series:

$$h_{eq_{series}} = \frac{1}{\sqrt[3]{\sum_{i=1}^{n} \frac{l_i}{l}\left(\frac{1}{h_i^3 \times \cos\theta_i}\right)}} \qquad (24)$$

Here, l_i is the projected length of the ith fracture member along the direction of the macroscopic pressure gradient axis, h_i and θ_i are aperture and inclination angle of the ith member respectively. The principal of deriving this expression is essentially same as that of deriving *Equation (18)*, and for all $\theta_i = 0$, it reduces to *Equation (18)*. Simulations were run (results not presented in this paper) in series fractures having one or several inclined members, and it was found that *Equation (24)* had excellent agreement with h_{eq} derived from simulation.

3.3.4 Effect of Fracture Orientation in a Parallel Network

In the case of parallel combination of fractures having arbitrary orientations, the total flow rate through the system is simply the sum of all flow rates through individual members, and the formula to compute h_{eq} can be written as follows:

$$h_{eq_{parallel}} = \sqrt[3]{\sum_{i=1}^{n}\left(h_i^3 \times \cos\theta_i\right)} \qquad (25)$$

This equation is nothing but a more general form of *Equation (16)*, and was verified to match simulation results quite well.

3.4 Flow Simulation in Fracture Networks

Fractured reservoir flow simulation, an application area that we are mainly interested in, requires modeling fluid flow in fracture networks. In most cases these fracture networks are formed by intersecting, oriented fractures. The reservoir models used in flow simulation are simplified representation of the actual geology of the fractured medium. The simplification procedure depends on the length scale of fractures relative to the simulation grids/blocks and also on the connectivity of those fracture sets. A schematic diagram showing some of the typical fractured reservoir models and the pertinent simulation schemes that are being used in the petroleum industry is given by *Figure 16*.

We present a simulation study in a model fracture network (*Figure 17*) in order to delineate flow in fracture networks. The complexity of the fracture network modeled in this study is comparable to the fractured

reservoir models used in real applications (e.g. medium to large scale connected fractures that use dual-porosity scheme as shown by *Figure 16*).

On *Figure 18*, we show the mesh from some of the zones of the network model. We took advantage of the flexible and adaptive meshing capacity of the Pre-Processor that we used and tried our best to create a balance between overall mesh quality and computational cost. For example, in many places we used non-uniform meshing by putting more mesh in the boundary layers of the channels and in the intersections than the other parts of the channel. As shown by *Figure 18*, both *quadrilateral* and *triangular* mesh elements were used in the computational model. This was done in order to keep the '*skewness*' of the meshes at a minimum possible level so that it would not adversely affect the convergence during flow simulation.

The steady-state simulation results from same parts of the network are plotted on *Figure 19*. These plots enable us to visualize the complexity of flow in networks.

The flow simulation in this fracture network yields a volumetric flow rate, $Q = 2.51 \times 10^{-5}$ m^3/s for a total pressure drop of 625 Pa ($P_{inlets} = 200625$ Pa, $P_{outlets} = 200000$ Pa) existing over a 0.5 m length in the x-direction (direction of pressure gradient axis). With these, we can characterize this network with the concept of equivalent hydraulic aperture: $h_{eq} = 1.06$ mm (by *Equation 15*). This essentially means that the steady-state flow response of this network will be the same as having a single 0.5 *m* long, 1.06 *mm* aperture, simple parallel-plate fracture oriented horizontally and subjected to a pressure differential of 625 *Pa* in a 0.5 *m* long reservoir grid block. It is noted that the magnitude of h_{eq} is very close to the true aperture of fracture *c* – this is because fracture *c* provides the easiest pathway for fluid all the way from inlet to outlet in the network, and so most of the flow is along this path, while others contribute very little.

In an effort to further our understanding in network fracture flows, we perturbed the given network by – (A) Increasing the aperture of fracture *f* by a factor of 2, (B) Increasing the aperture of fracture *a* by a factor of 4, and (C) Adding a straight fracture of *2 mm* aperture to the network in the upper part that extends all the way from inlet to outlet. For each case, we did flow simulation and computed h_{eq} from the simulation results. In cases (A) and (B), increments in h_{eq} were insignificant (*1.07 mm* and *1.1 mm* respectively) compared to the original network, but in case (C) a drastic change in the velocity and pressure distribution was observed, along with a significant change in h_{eq} (2.17 mm).

From these, we conclude that in a network of intersecting fractures, the fracture that cuts across the boundaries (inlet and outlet) and has the smallest inclination with respect to the pressure gradient axis will serve as the least resistive path to fluid and therefore will carry most of the flow in the network; also the equivalent hydraulic aperture of the network will have a magnitude close to (and larger than) the aperture of that fracture.

3.5 Comparison Between *Stokes* and *Navier-Stokes* Simulation

Flow simulation using *Stokes* equation is much simpler and computationally less expensive than using full *Navier-Stokes* equation. But Stokes equation is only valid for very slow flow. In this section, we use a series fracture model [{li, hi} = {3 cm, 2 mm}, {3 cm, 0.4 mm}, {3 cm, 1.4 mm}] to determine at what ranges of *Re* the hydraulic characterization of fractures using both methods are comparable. For *Stokes* flow simulation, we use an in-house developed code (Sarkar *et al*. 2002), and for *Navier-Stokes* simulation we use the commercial package that is used for all other simulations presented on this paper. As seen from *Figure 20*, for both low and (moderately) high *Re*[6] cases, the *Stokes* method forces the simulator to form fully-developed velocity profiles in each fracture section. *Navier-Stokes* simulation also yields very similar uniform profiles for low *Re* case (*Figure 21(a)*), but as *Re* increases, the advective terms come into play and some vortices start to form near the sharp corners of the fracture (last section of the fracture, as seen on *Figure 21(b)*). In real fractures, where surfaces are rough and rugose, and geometry change can be abrupt, eddies like these may occur even at fluid velocities lower than the threshold magnitude required for the onset of turbulent flow. It was found, however, that these "non-linearities," especially at

---

[6] *Re* reported for these models are calculated based on the inlet mean velocity. In our case, for the same pressure gradient *Stokes* and *Navier-Stokes* simulation will yield slightly different inlet velocity profiles; hence *Re* would be slightly different too. These differences are quite normal, because the numerical algorithm and gridding schemes used by these methods are very different.

low *Re* values, do not make much difference in the equivalent hydraulic conductivity magnitudes (*Figure 22*). Based on this observation we conclude that, both methods (*Stokes* or *Navier-Stokes*) will give satisfactory and comparable hydraulic parameter estimates for *Reynolds number* magnitude upto 100 (*0 < Re < 100*). This probably covers most part of conceivable viscous, incompressible fluid flow in subsurface fractures at reservoir conditions – far from well-bore. The upper limit of *Re* for *Stokes* method to be valid will depend on how geometries change along the fracture: the cutoff number will be much less for fractures with higher amplitude higher frequency wall asperity variations than relatively smooth fractures.

3.6 Flow Simulation in Fractures with Rough Surfaces

At low flow velocities, the two main causes of deviations from the *Cubic law* are roughness of the fracture walls and asperity contact[7] between the opposing fracture faces. In this section we present a 2D simulation in a fracture with rough surface. Flow simulation rough surfaces fractures are more suitable for laboratory scale analysis of rock fractures than reservoir scale treatment of fractures.

Rough surface fracture models for our study are generated by using the mathematical model proposed by Brown (1995). We first determined the appropriate set of modeling parameters by upscaling the values that are reported by Brown (1995), and used them to generate two 3D fracture surfaces at a length scale of our interest. (A sample 3D surface is shown by *Figure 23*). Then we made some adjustments between the separations of the two surfaces to ensure that they did not touch each other at any location. (Flow simulation in fractures with asperity contacts will be discussed later). Finally we took a 2D section and thus prepared our fracture geometry for flow simulation. Some results from our flow simulation are shown by *Figure 24*.

The overall length (horizontal distance between inlet and outlet) for this model is 80 cm. We found $Q = 6.21x10^{-5} m^3/s$ for an overall pressure differential $\Delta P = 870.8 Pa$ existing between inlet and outlet. (Pockets of relatively high velocity are observed at constrictions/narrow aperture sections). Next, *Equation (15)* was used to compute the equivalent hydraulic aperture for this model, yielding h_{eq} = 1.51 mm. For realistic fractures with high frequency variation of apertures, doing a flow simulation is the most reliable method for estimating equivalent hydraulic parameters. Alternatively, one can approximate this rough fracture with *n* numbers of serially connected small parallel-plate fracture segments (the concept of *Figure 8*), and then use the formula for serial combination of fractures to estimate the equivalent hydraulic aperture. To show how this can be accomplished, we also sampled the aperture values at equal (length) intervals over the entire fracture to obtain 513 aperture samples (representing 513 fractures connected in series, each having equal lengths). The minimum, maximum, mean and std. of these samples are (in *mm*): 0.56, 5.19, 2.12, and 0.859 respectively. Using equal length fraction for each fracture, i.e. l_i/l = 1/513, the equivalent hydraulic aperture is estimated by Equation (18) as *1.54 mm*. This is indeed in good agreement with the value obtained from flow simulation (h_{eq} = 1.51 mm).

3.7 Flow Simulation in 3D

Real fractures are 3D. Although insights about the fluid motion can be gained by studying 2D models, to understand the actual flow occurring in natural fractures, 3D modeling is essential. Examples from our 3D simulation are summarized in the following.

3.7.1 Brick-shaped fracture

This is simply an extension of the 2D parallel plate model in the direction perpendicular to the 2D fracture plane. In our 2D models, we assumed the width very large compared to the aperture; however in 3D representation it has a finite width. *Figure 25* shows the 3D model and plots some simulation results. The model dimensions are: length (x) = 5 cm, width (y) = 5 cm, aperture (z) = 2 mm. For a pressure differential between inlet and outlet $\Delta P = 0.76 Pa$, we obtained a volumetric flow rate, $Q = 1x10^{-7} m^3/s$ for this 3D model. The velocity profile is parabolic; however it gradually flattens and becomes zero as it approaches the walls. This '*edge*' or '*wall*'

---

[7] To properly understand the effects of asperity contacts, full 3D modeling is required, because in 2D analysis, asperity contacts will result in flow blockage, however in reality (3D) flow may still continue around those obstructions.

effect can be clearly seen by the flattening/dampening of velocity vectors near the walls (*Figure 25(c)*). The velocity profile, u(y,z), from simulation has excellent agreement with the analytical form (*Figure 26*).

3.7.2 Flow Model with variable aperture

This is also a 3D extension of one type of the series models studied in 2D. The properties of this 3D model are: length (x) = 5 cm, width (y) = 5 cm, and apertures (z_i) = 2 mm, 0.5 mm & 1 mm. The model and some simulation results are plotted on *Figure 27*. Q = 1×10^{-7} m^3/s is computed for an overall pressure drop ΔP = 15.2 Pa. Overall pressure gradient in the flow model is linear and uniform, similar to the brick-shaped model, however some localized non-linearity is seen at the intersections /sharp corners where fracture geometries change (*Figure 27[c & d]*). The concept of *equivalent hydraulic aperture* that we used in 2D can be also applied in 3D, and the 3D steady-state simulation results can be used to characterize the hydraulic conductivity of a 3D fracture in the following manner:

$$h_{eq_{simulation}} = \sqrt[3]{\frac{12 Q_{simulation} \mu l}{W(P_i - P_o)}} \qquad (26)$$

Theoretical expressions for computing h_{eq} for series and parallel network of 3D fractures can also be devised as follows:

$$h_{eq_{series}} = \frac{1}{\sqrt[3]{\sum_{i=1}^{n} \left[\frac{W}{W_i} \times \frac{l_i}{l} \left(\frac{1}{h_i^3} \right) \right]}} \qquad (27)$$

$$h_{eq_{parallel}} = \sqrt[3]{\sum_{i=1}^{n} \left(\frac{W_i}{W} \times h_i^3 \right)} \qquad (28)$$

where, W_i is the width of the ith 3D fracture, and W is the width of the equivalent 3D block that we wish to use in replacement of n individual fractures.

For the *Case 3d.2* presented here, $h_{eq_{simulation}}$ = *0.734 mm*, while theoretically, $h_{eq_{series}}$ = *0.714 mm*. A possible explanation for this slight discrepancy is that *Equation 26* is actually an approximate rather than exact relation in view of 3D flow. *Equation 26* is just another form of *Equation 7*, which basically states that the volumetric flow rate per unit width through a 2D model can be multiplied with a width W to give the volumetric flow rate through its 3D counterpart. In reality, however, this multiplication will result in an overestimation of the actual 3D flow rate, because in real 3D flow there will be that 'wall' or 'edge' effect as was shown by *Figure 25(b)*. However, when W is much larger than h, the wall effect may be considered negligible, and it is safe to use *Equation 26*.

3.7.3 Fracture model with asperity contacts

The previous two 3D models were simple in a sense that each of them could be replaced with a 2D model and simulation could be carried out in 2D without much loss or accuracy. In fact, for transversely isotropic models, which are very often used in seismic modeling of fractures, 3D flow models can be replaced with equivalent 2D models in order to save the cost of computation. However, when the roughness of fracture surfaces are considered important in flow modeling, a full 3D simulation is essential. In this section, we show a slightly complicated 3D fracture model with varying apertures (asperity) and presence of asperity contacts (*Figure 28*). *Navier-Stokes* simulation can be used to study flow distribution around obstructions (Figure 29). The steady-state volumetric flow rate obtained for this 3D fracture is Q = 1×10^{-7} m^3/s, for ΔP = 6.579 Pa between the inlet and outlet. With this information, the equivalent hydraulic aperture for this 3D fracture model can be computed as:

$$h_{eq} = \sqrt[3]{\frac{12 Q \mu l}{W(P_i - P_o)}} = \sqrt[3]{\frac{12 \times 1e-7 \times 0.005 \times 0.05}{0.05 \times 6.579}} \cong 0.97 mm$$

The numerical model of this 3D object consists of a total 705243 computational cells (control volumes). It is not possible to determine the series/parallel connection of these cells, and therefore no theoretical formula can be used in such cases to predict/estimate h_{eq}. The minimum, average (mean), and maximum values of these cell heights are *0.008 mm*, *0.1015 mm*, and *0.1919 mm* respectively, however nothing conclusive can be said about the h_{eq} from these values. Therefore, doing a Computational Fluid Dynamics based flow simulation is the most reliable, and perhaps the only way to provide estimates of equivalent hydraulic parameters for real 3D fractures.

4.   Conclusion

The simplicity of *cubic law* in computing fracture *transmissivity* (or *permeability*) makes it a popular choice among the reservoir simulation community. We recommend using a modified cubic law, namely "*generalized cubic law*" that relates *fracture transmissitvity* (or *permeability*) to the *equivalent hydraulic aperture* of a fractured medium. In this paper, we proposed methods for computing *equivalent hydraulic aperture* for different types of fracture models.

Numerical solutions of either *Stokes* or *Navier-Stokes* equation can be used to model slow flow of viscous and Newtonian fluids (e.g. oil, water) in subsurface fractures. *Navier-Stokes* is more reliable especially when modeling flow in variable aperture or rough fractures; however based on our analysis in a few fracture models, we conclude that *Stokes* equation based modeling yields comparable hydraulic property estimates for *Reynolds numbers* upto approximately 100. This upper limit, though, will vary depending on the severity and frequency of aperture variation in the fracture.

To estimate the *equivalent hydraulic aperture*, a flow simulation in the fracture is preferred. In fact, for complicated 3D fracture geometries, or for complex 2D/3D fracture networks, flow simulation may be the only way to estimate the true *equivalent hydraulic aperture* of the fractured medium. However, when the fracture geometry is not known to build the computational model or due to other constraints a complete flow simulation cannot be performed, the following rules will serve as good alternatives in estimating *equivalent hydraulic apertures*: 1) For series fractures, using the harmonic mean of all apertures cubed, 2) For parallel fractures, using the sum of all apertures cubed, 3) For rough surface fractures, modeling it as a series combination of several parallel-plate fractures using the surface roughness information, 4) For inclined fractures, using a *cosine* correction term, 5) For fracture networks, using the aperture of the fracture that offers the shortest continuous path from inlet to outlet.

The methodology described in this paper is very robust and using this method insights were gained about the relative significance of some major fracture flow controlling factors such as *aperture*, *length*, *constriction*, *width*, *asperity contacts*, *orientation*, and *intersection*. Work is currently underway to apply the method and results described in this paper to a reservoir problem.

Reference

Adler, P.M., and Thovert, J.-F.: 1999, *Fractures and Fracture Networks*, Kluwer Academic Publishers, Dordrecht.

Barenblatt, G.I, Zheltov, Iu P., and Kochina I.N.: 1960, "Basic Concepts in the Theory of Seepage of Homogeneous Liquids in Fissured Rocks", *J. Appl. Math.* **24**, 1286.

Barth, T.J. and Jespersen, D.: 1989, "The design and application of upwind scheme on unstructured meshes", *Technical Report AIAA-89-0366*, AIAA 27th Aerospace Sciences Meeting, Reno, Nevada.

Brodkey, R.S.: 1967, *The Phenomenon of Fluid Motions*, Addison-Wesley Publishing Company.

Bourbiaux, B., Basquet, R., Cacas, M-C., and Daniel, J-M.: 2002, "An Integrated Workflow to Account for Multi-Scale Fractures in Reservoir Simulation Models: Implementation and Benefits", *paper SPE 78489* presented at the 10th Abu Dhabi International Petroleum Exhibition and Conference.

Brown, S.R.: 1995, "Simple mathematical model of a rough fracture", *J. Geophys. Res*. **100**, 5941-5952.

Cacas, M.C., Daniel, J.M., and Letouzey, J.: 2001, "Nested Geological Modeling of Naturally Fractured Reservoirs", *Petroleum Geoscience*, Vol. **7**, pp. S43-S52.

Chung, T.J.: 2002, *Computational Fluid Dynamics*, Cambridge University Press.

Committee on Fracture Characterization and Fluid Flow: 1996, *Rock Fractures and Fluid Flow: Contemporary Understanding and Applications*, National Academy Press.

Consentino, L., Coury, Y., Daniel, J.M., Manceau, E., Ravenne, C., van Lingen, P., Cole, J., and Sengul, M.: 2001, "Integrated Study of a Fractured Middle East Reservoir with Stratiform Super-K Intervals – Part 2: Upscaling and Dual Media Simulation", *paper SPE 68184* presented at the 2001 SPE Middle East Oil Show held in Bahrain, March.

Damsleth, E. and Sangolt, V.: 1998, "Sub-seismic faults can seriously affect fluid flow in the Njord field off Western Norway – A stochastic fault modeling case study", *paper SPE 49024*, presented at the SPE Annual Technical Meeting and Exhibition, New Orleans, Louisiana, 295-304.

de Marsily, G.: 1986, *Quantitative Hydrogeology,* Academic Press, San Diego, California.

Dershowitz, B., LaPointe, P., Eiben, T., and Wei, L.L.: 2000, "Integration of Discrete feature netwok methods with conventional simulator approaches", *SPE Reservoir Evaluation and Engineering*, v. 3, pp. 165-170.

Ertekin, T., Abou-Kaseem, J.H., and King, G.R.: 2001, *Basic Applied Reservoir Simulation*, SPE Text Book Series Vol. 7, Richardson, Texas.

Gauthier, B.D.M. and Lake, S.D.: 1993, "Probabilistic modeling of faults below the limit of seismic resolution in Pelican Field, North Sea, offshore United Kingdom", *AAPG Bulletin*. **77**, 761-777.

Gursul, I.: 1998, "Incompressible Laminar Viscous Flows", *In*: Johnson, R.W. (ed) *The Handbook of Fluid Dynamics*, CRC Press.

He, N., Lee, S.H., and Jensen, C.L.:2001, "Combination of Analytical, Numerical and Geostatistical Methods to Model Naturally Fractured Reservoirs", *paper SPE 68832* presented at the SPE Western Regional Meeting held in Bakersfield, CA, March.

Henn, N., Bourbiaux, B., Quintard, M., and Sakthikumar, S.: 2000, "Modeling Fluid Flow in Reservoirs Crossed by Multiscale Fractures: A New Approach", *paper presented at the 7th European Conference on the Mathematics of Oil Recovery*, Baveno, Italy, September.

Holmes, D.G. and Connell, S.D.: 1989, "Solution of the 2D Navier-Stokes Equations on Unstructured Adaptive Grids", presented at the *AIAA 9th Computational Fluid Dynamics Conference*.

Huitt, J.L.: 1955, "Fluid Flow in Simulated Fractures," *Amer. Inst. Chem. Eng. Journal*, vol. **2**, pp. 259-264.

Issa, R.I.: 1986, "Solution of the Implicitly Discretised Fluid Flow Equations by Operator-Splitting", *J. Comput. Phys.*, Vol. **62**, pp. 40-65.

Jourde, H., Flodin, E.A., Aydin, A. Durlofsky, L.J., and Wen, X-H.: 2002, "Computing Permeability of Fault Zones in Eolian Sandstone from Outcrop measurements", *AAPG Bulletin*, V. **86**, pp. 1187-1200.

Kazemi, H., Merrill, L.S., Porterfield, K.L, and Zeman, P.R.: Dec. 1967, "Numerical Simulation of Water-Oil Flow in Naturally Fractured Reservoirs", *SPE Journal*. 317.

Koudine, N., Gonzalez Garcia, R., Thovert, J.-F., and Adler, P.M.: 1998, "Permeability of Three-Dimensional Fracture Networks", *Physical Review E*, **57**, No. 4.

Lisle, R.J.: 1994, "Detection of zones of abnormal strains in structures using Gaussian curvature analysis", *AAPG Bulletin*. **78**, 1811-1819.

Lough, M.F., Lee, S.H., and Kamath, J.: 1997, "A New Method to calculate the Effective Permeability of Grid Blocks Used in the Simulation of Naturally Fractured Reservoirs", *SPERE*, 219-224, Aug.

Madden, T.R.: 1976, "Random Networks and Mixing Laws", *Geophysics*. 41, 1104-1125.

Nelson, R.A.: 2001, *Geological Analysis of Naturally Fractured Reservoirs*. Gulf Professional Publishing.

Parsons, R.W.: 1966, "Permeability of Idealized Fractured Rock", *Soc. of Petroleum Engineers Journal*, pp. 126-136, June.

Patankar, S.V.: 1980, *Numerical Heat Transfer and Fluid Flow*, Hemisphere Publishing Corporation, Taylor & Francis Group, New York.

Paterson, A.R.: 1983, *A First Course in Fluid Dynamics*, Cambridge University Press.

Sarkar, S., Toksöz, M.N., and Burns, D.R.: 2002, "Fluid Flow Simulation in Fractured Reservoirs", *Report, Annual Consortium Meeting*. MIT Earth Resources Laboratory.

Sarda, S., Bourbiaux, B., Cacas, M.C., and Sabathier, J.C.: 1997, "A Fast and Efficient Methodology to Convert Fractured Reservoir Image into a Dual-Porosity Model", *paper SPE 38907* presented at the SPE ATCE, San Antonio, TX, Oct.

Sarda, S., Jeannin, L., Basquet, R. and Bourbaux, B.: 2002, "Hydraulic Characterization of Fractures Reservoirs: Simulation on Discrete Fracture Models", *SPE Formation Evaluation*, April.

Sherman, F.S.: 1990, *Viscous Flow*, McGraw-Hill Publishing Company.

Snow, D.T.: 1965, "A Parallel Plate Model of Fractured Permeable Media," *Ph.D. Dissertation*, University of California.

Thomas, L.K., Dixon, T.N., and Pierson, R.G.: 1983, "Fractured Reservoir Simulation", *SPE Journal*, Feb., 42-54.

van Golf-Racht, T.D.: 1982, *Fundamentals of Fractured Reservoir Engineering*, Developments in Petroleum Science, no. 12, Elsevier Scientific Publishing Company, Netherlands.

Versteeg, H.K. and Malalasekera, W.: 1995: *An Introduction to Computational Fluid Dynamics: The Finite Volume Method*, Prentice Hall.

Warren, J.E., and Root, P.J.: Sept. 1963, "The Behavior of Naturally Fractured Reservoirs", *SPE Journal*. 245.

Wilkes, J.O.: 1999, *Fluid Mechanics for Chemical Engineers*, Prentice Hall.

Witherspoon, P.A., Wang, J.S.Y., Iwai, K. and Gale, J.E.: 1980, "Validity of Cubic Law for Fluid Flow in a Deformable Rock Fracture", *Water Resour. Res*. **16**, 1016-1024.

Wu, Y-S., and Pruess, K.: 2000, "Numerical Simulation of non-isothermal multiphase tracer transport in heterogeneous fractured porous media", *Advances in Water Resources*, **23**, pp. 699-723.

Zimmerman, R.W., and Bodvarsson, G.S.: 1996, "Hydraulic Conductivity of Rock Fractures", *Transport in Porous Media*. **23**, 1-30.
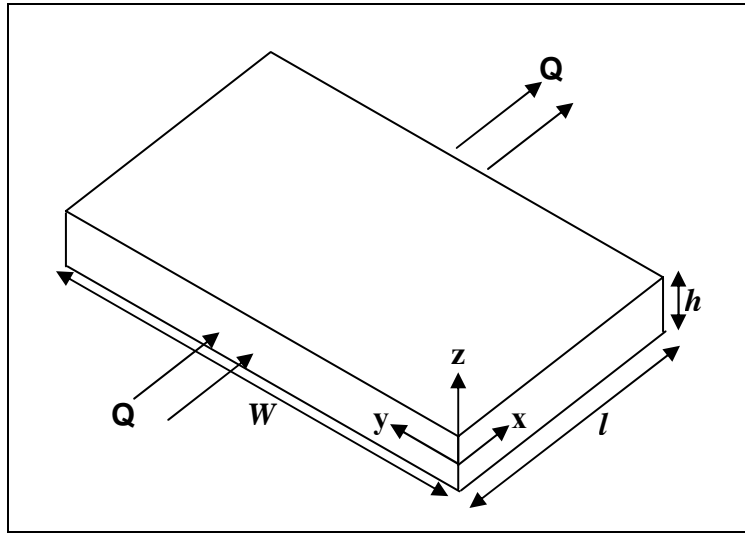
Figure 1: Parallel plate flow model for fractures.
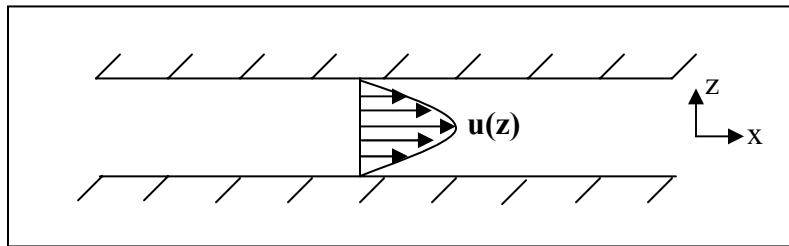
Figure 2: Parallel plate flow model in 2D, and the parabolic velocity profile.
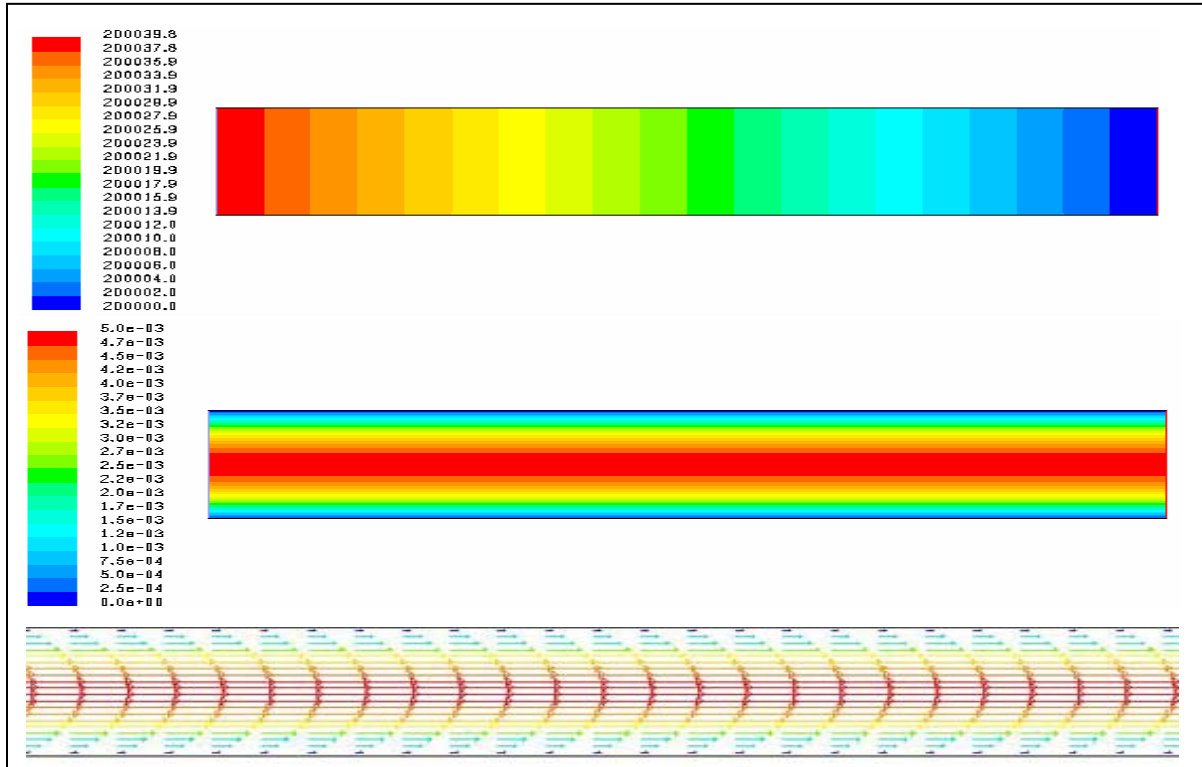
Figure 3: Flow simulation results in a parallel plate model. From top to bottom: pressure distribution (contours), velocity distribution (contours), velocity vectors showing a parabolic velocity profile.

20
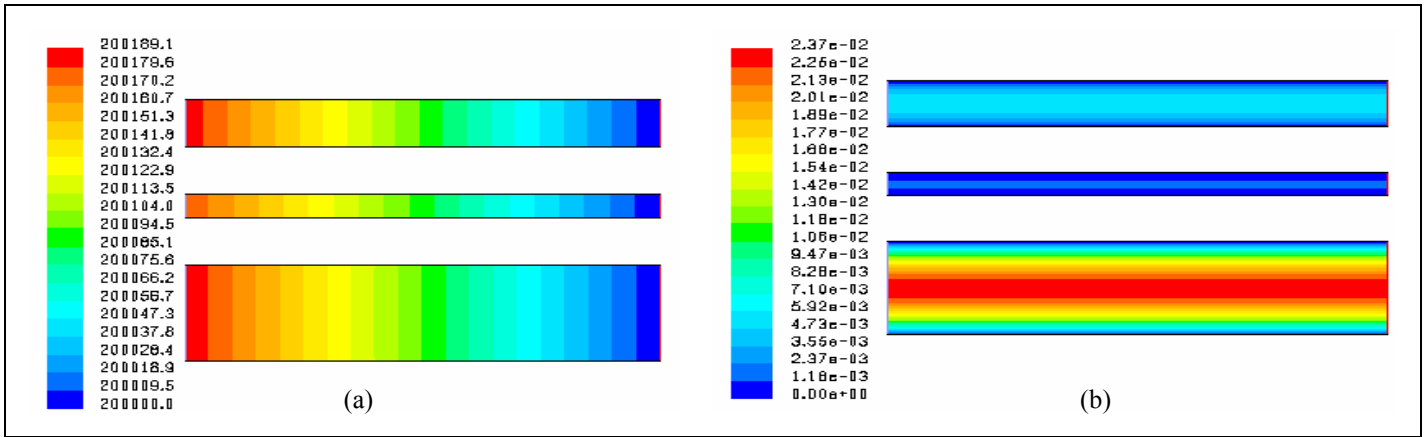
Figure 4: Flow simulation results for three distinct fractures connected in parallel: (a) Pressure Contours, and (b) Velocity Contours.
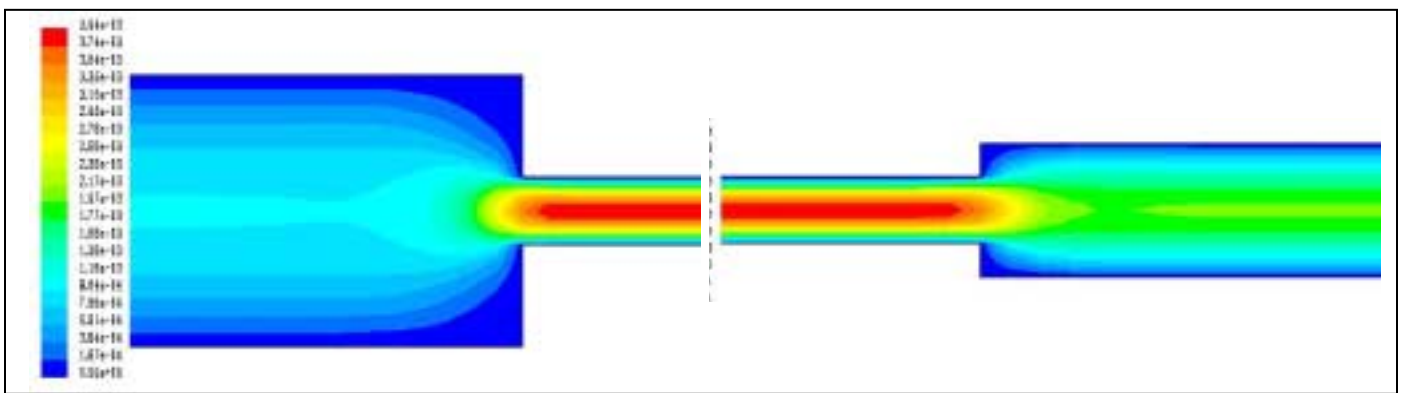
Figure 5: Velocity magnitude contours for *Case a*. (Model has very high aspect ratio, therefore to show undistorted velocity contours, only parts of the model are plotted.)
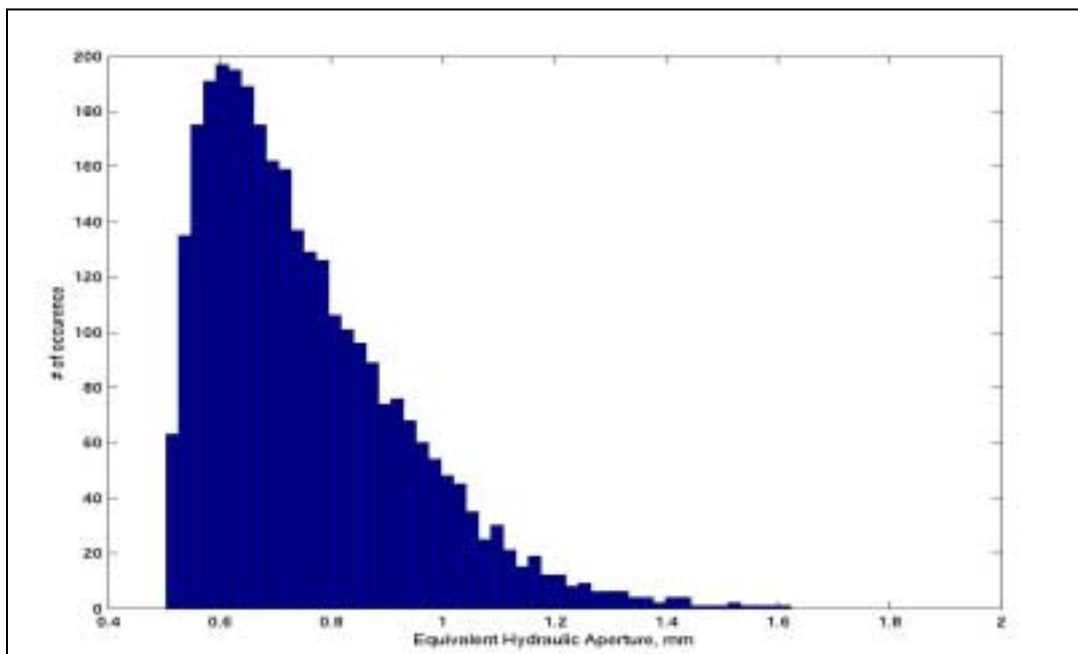
Figure 6: Histogram (plotted in 50 bins) of equivalent apertures for a series network with 3 discrete fractures having variable length fractions.

21
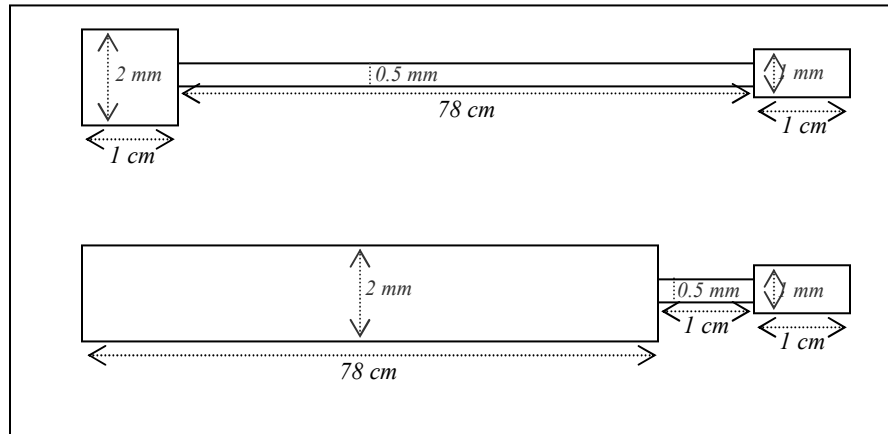
Figure 7: (For a total length of *80 cm)*: Upper – Series combination yielding minimum h_{eq};
Lower – Series combination yielding maximum h_{eq}.
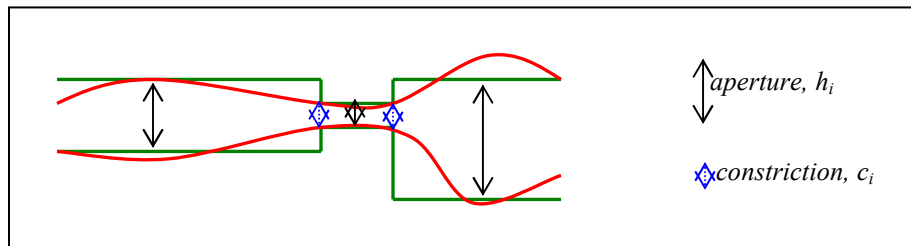
Figure 8: Approximating rough fractures with smooth, *parallel plate* models.
Lines in red indicate real fracture surfaces, lines in green indicate parallel
plate representation of those surfaces.
Terms 'aperture' and 'constriction' are defined as shown.
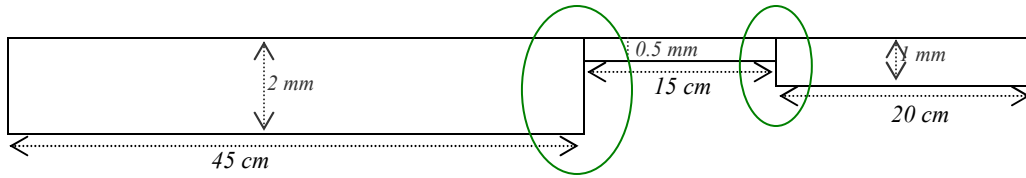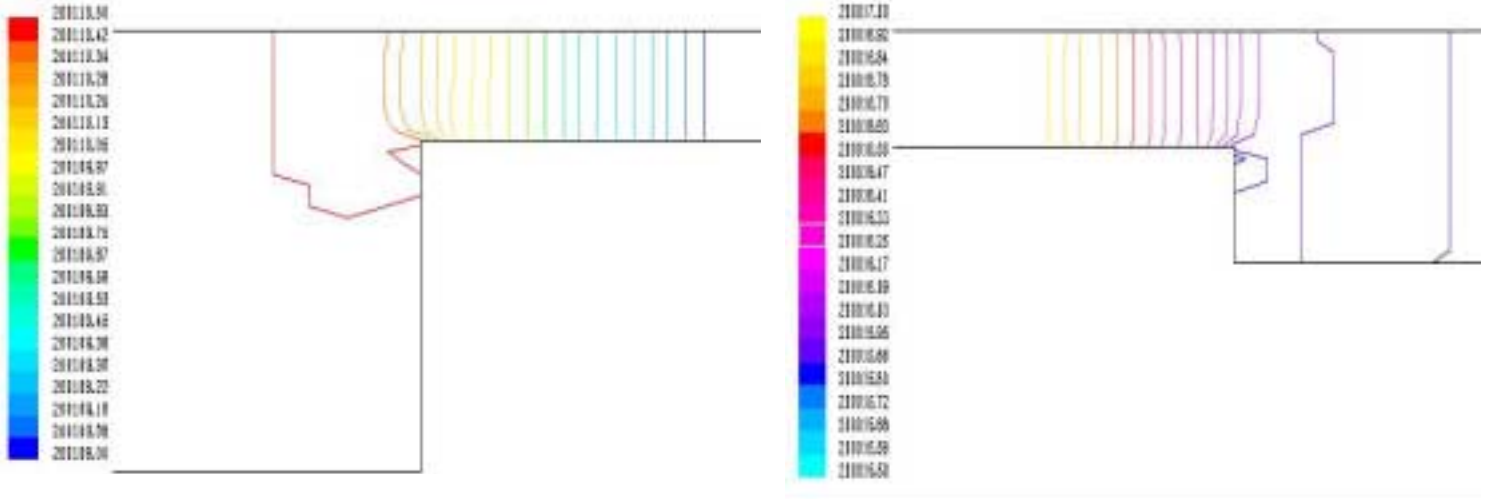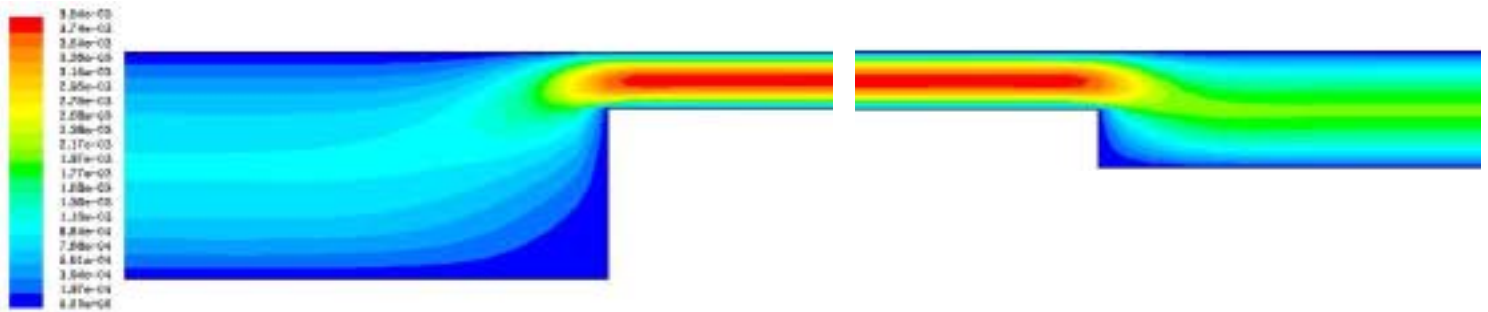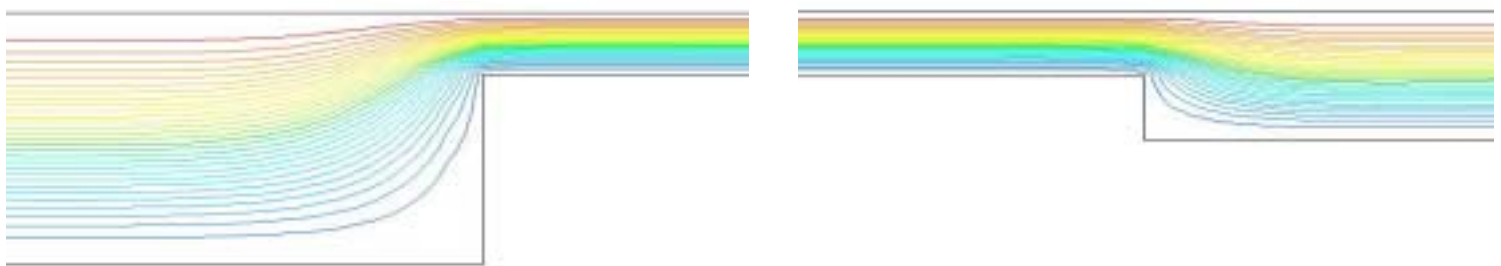
Figure 9: **[a]** Model geometry: the green ovals indicate regions for which simulation results are presented.
[b] (Un-filled) Pressure contours in regions identified by green ovals in [a]. Separate color-maps are used for two regions to better represent the variation of local contours. **[c]** (Filled) contours of Velocity magnitudes.
[d] (Un-filled) contours of Stream functions that extend from inlet to outlet.
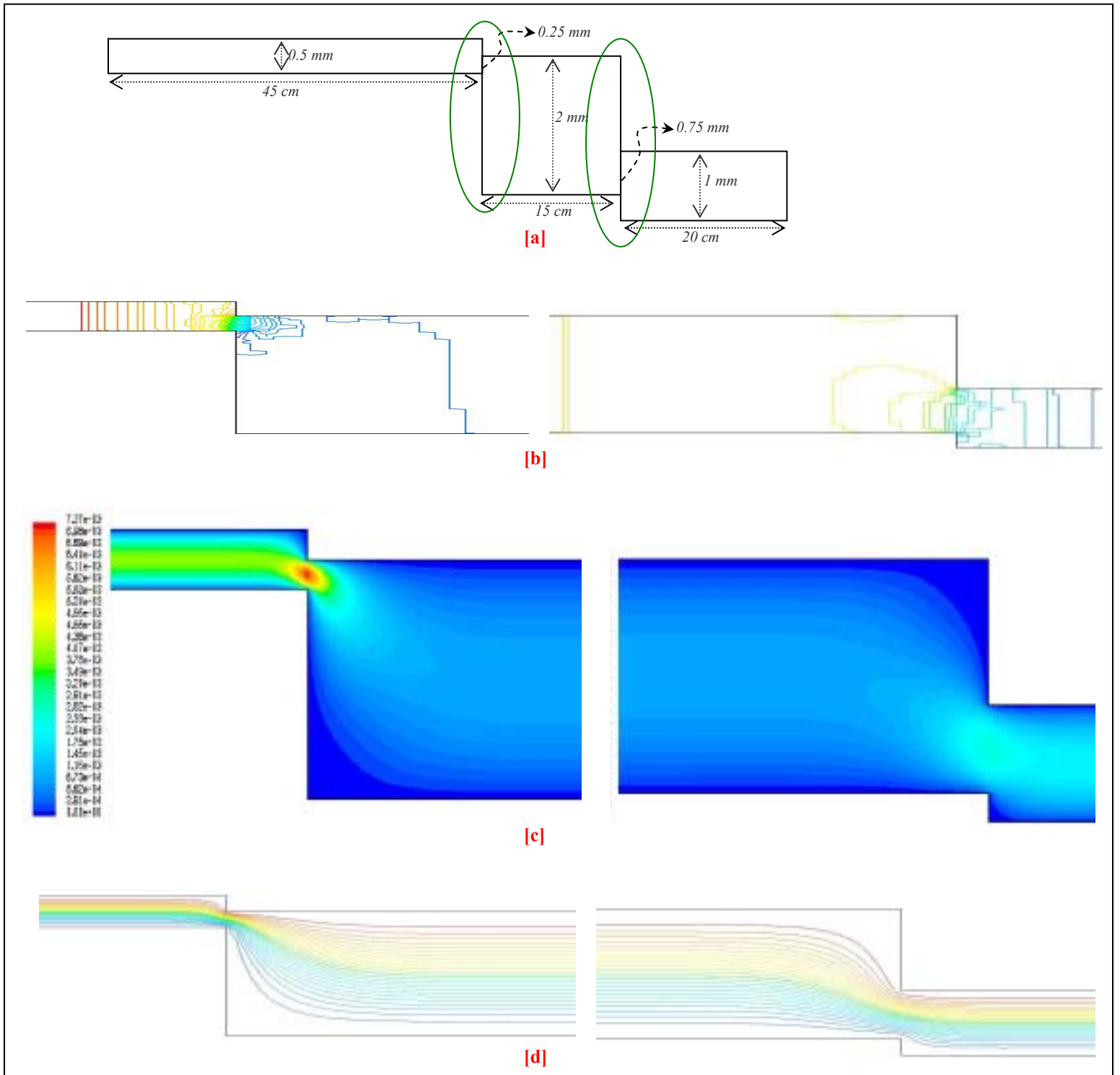
Figure 10: **[a]** Geometry of a fracture model, where the magnitude of constrictions are different than the magnitudes of adjacent apertures. The green ovals indicate regions for which simulation results are presented.
[b] (Un-filled) Pressure contours in regions identified by green ovals in [a] showing non-linearity due to constrictions. **[c]** (Filled) contours of Velocity magnitudes – large contrast in velocity magnitude at the constrictions.
[d] (Un-filled) contours of Stream functions that extend from inlet to outlet.
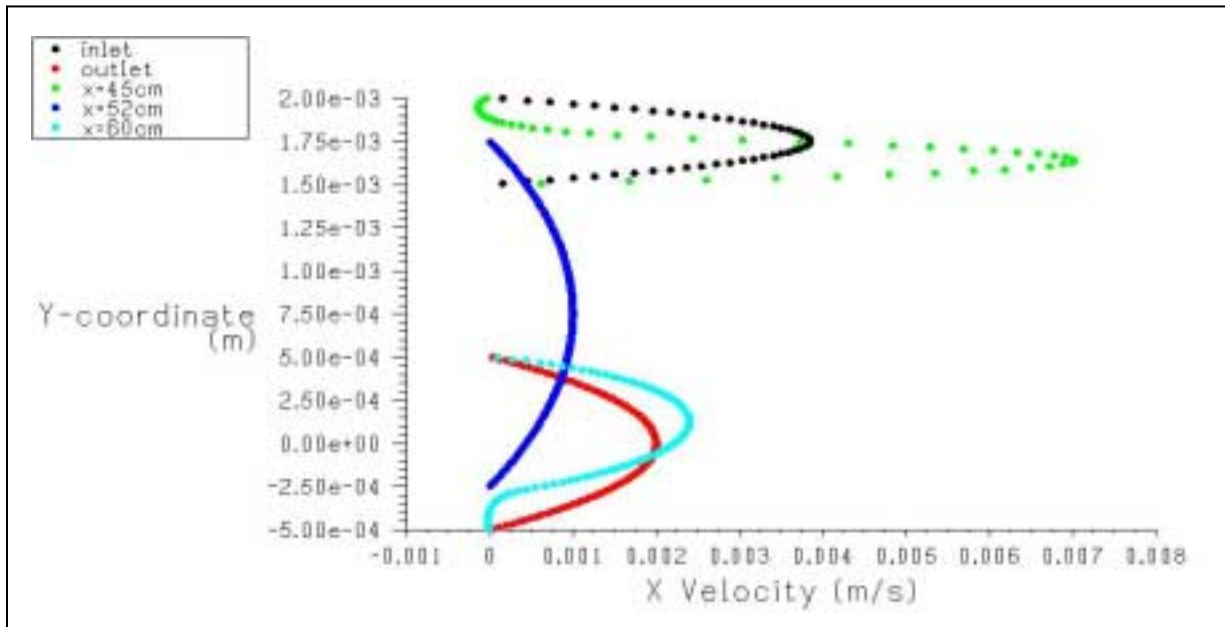
Figure 11: X-velocity magnitudes at different locations (constant x planes) for the model shown by *Figure 10[a]*. The constrictions are located at x=45 cm (green dots) and x=60 cm (sky blue dots). A sharp changed is noticed at x=45 cm compared to its adjacent fracture sections (black dots and dark blue dots). Velocity profile is parabolic in each section – a characteristic of laminar flow.
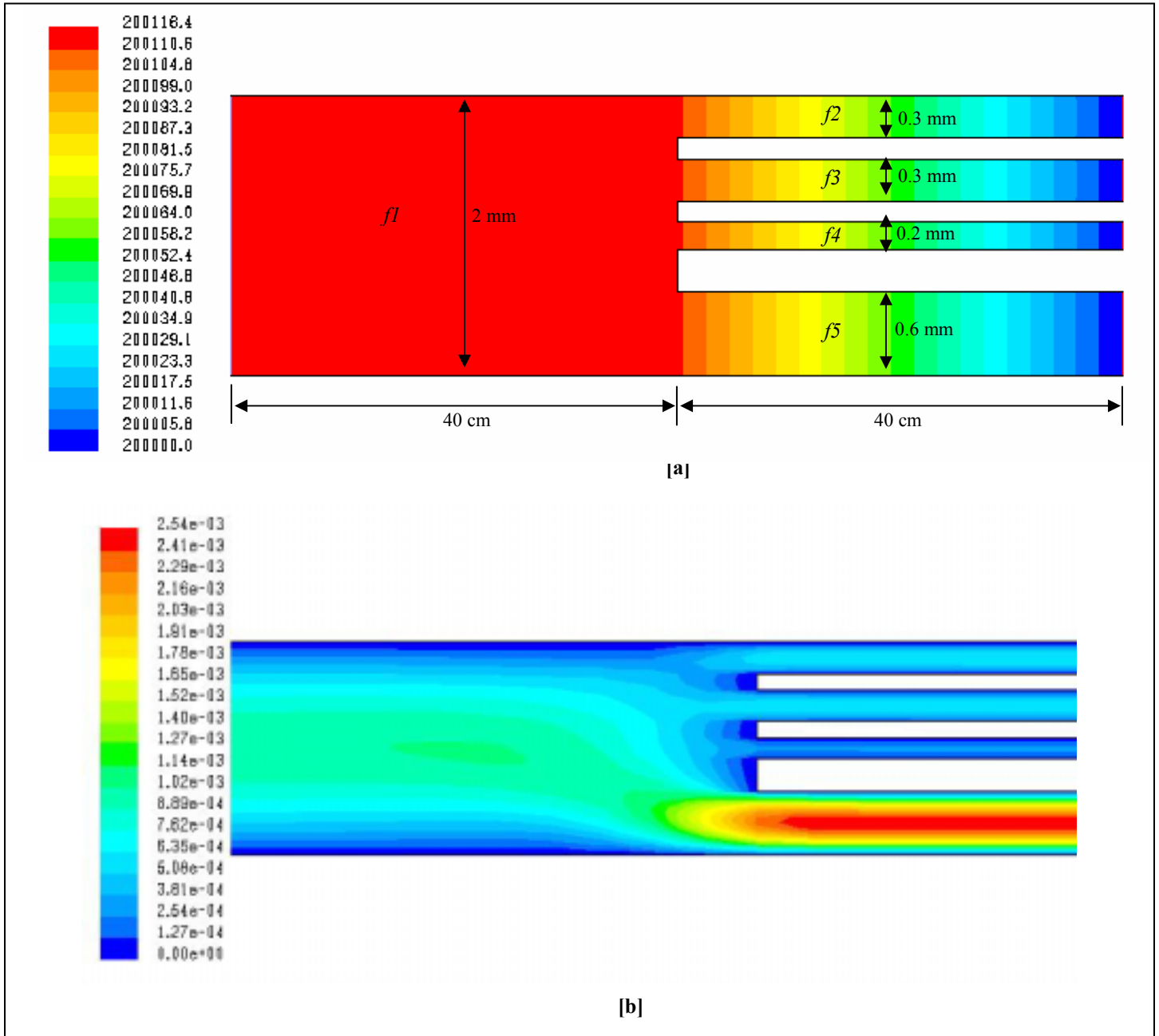
Figure 12: Combination of series and parallel fractures. **[a]** Pressure contours (also showing fracture dimensions). **[b]** Velocity contours near the intersections.
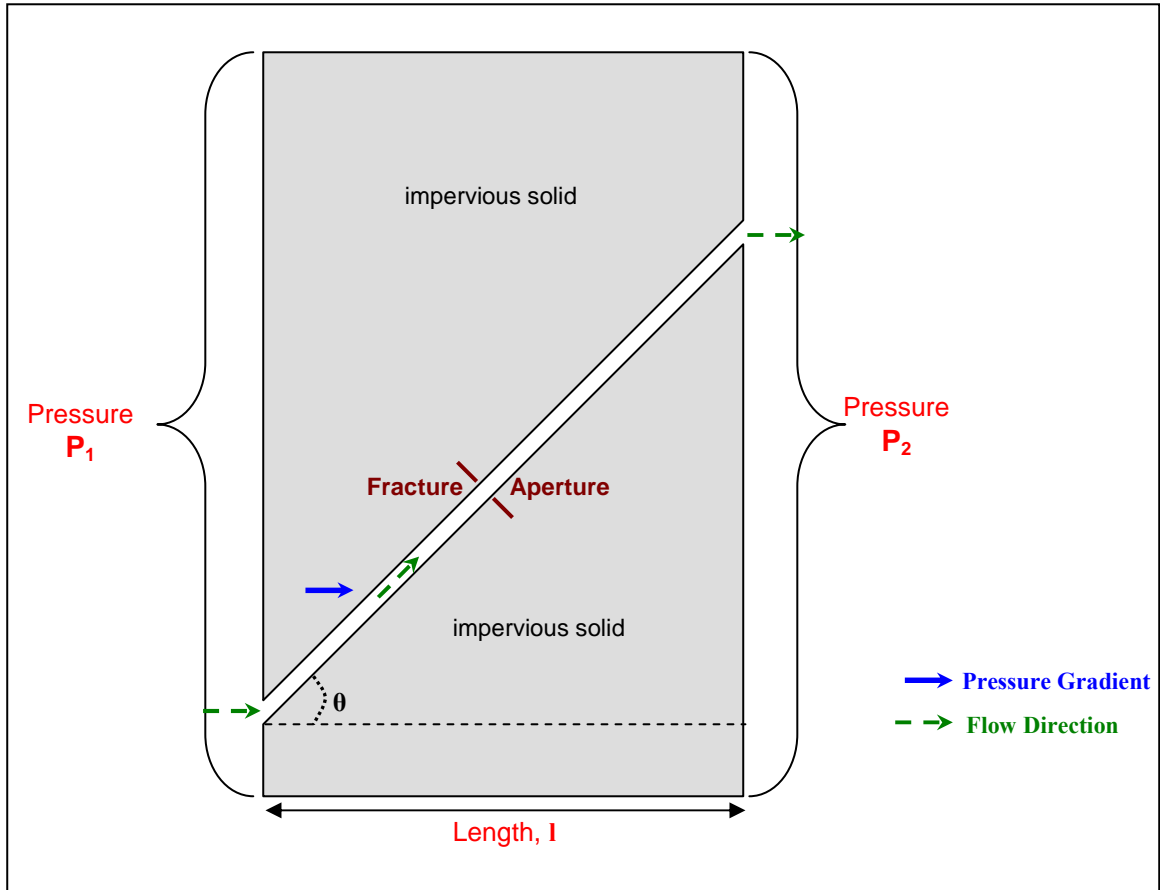
Figure 13: A fracture inside a rock slab, making an angle θ with the axis of overall pressure gradient, given by (P$_1$-P$_2$)/l.
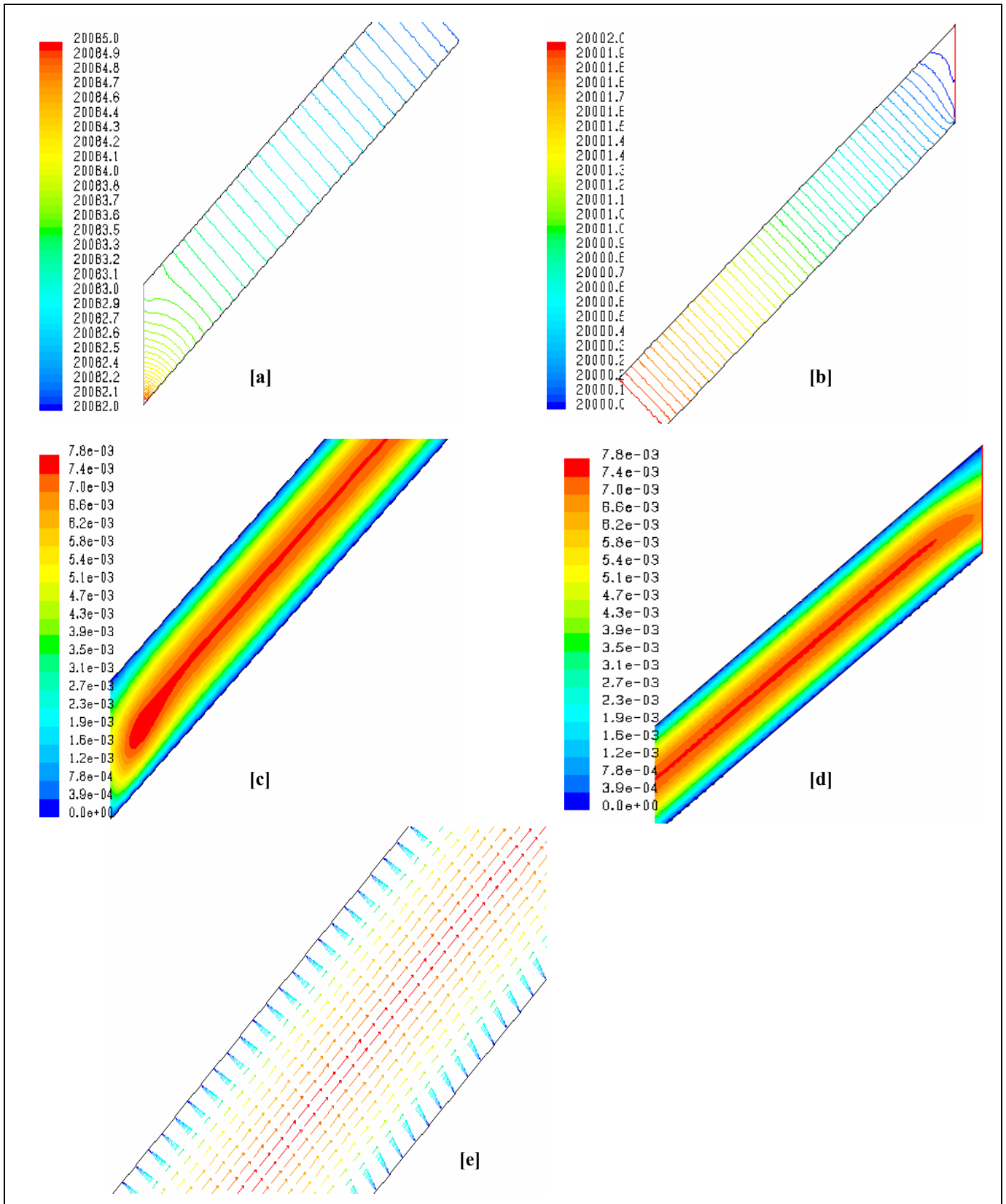
Figure 14: Flow in a 45° fracture. Pressure Contours: **[a]** near the Inlet, and **[b]** near the Outlet. Velocity Magnitude Contours: **[c]** near the Inlet, and **[d]** near the Outlet. **[e]** - Velocity vectors in the mid-zone, exhibiting a parabolic profile normal to the fracture cross-section.
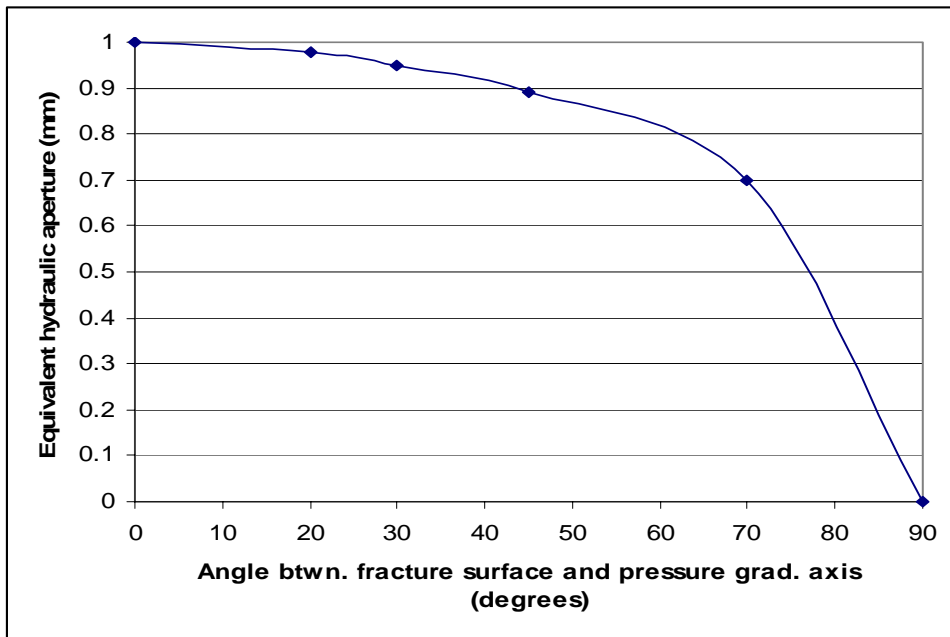
Figure 15: Effect of fracture inclination in hydraulic conductivity estimation. The plot is for inclination angle, θ vs. equivalent hydraulic aperture, h_{eq} $(= \sqrt[3]{h^3 \times \cos\theta}$)
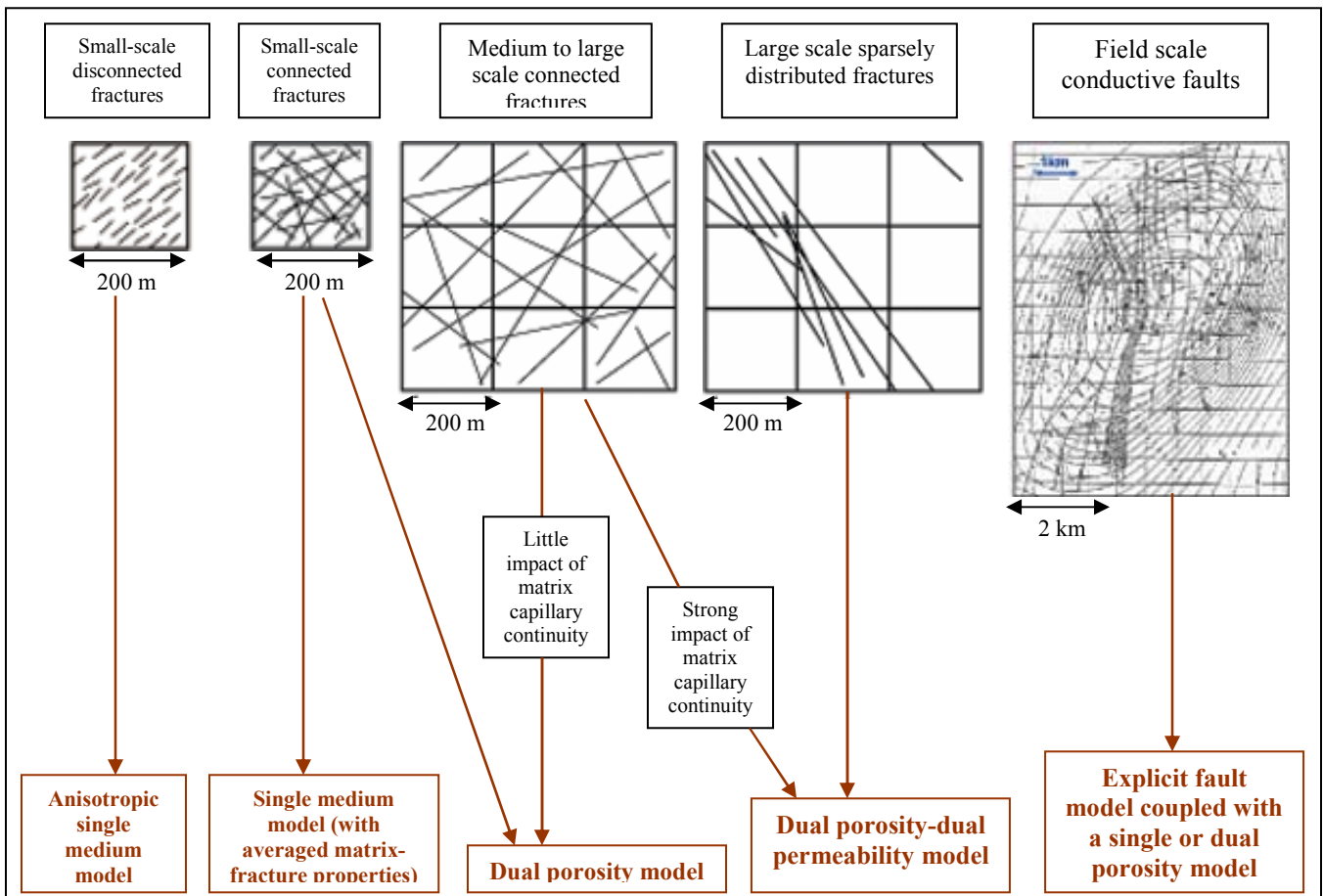
Figure 16: Methodology of choice for reservoir flow simulation models, depending on the length-scale of fractures relative to a reservoir grid-block (adopted from Bourbiaux *et al.* 2002).
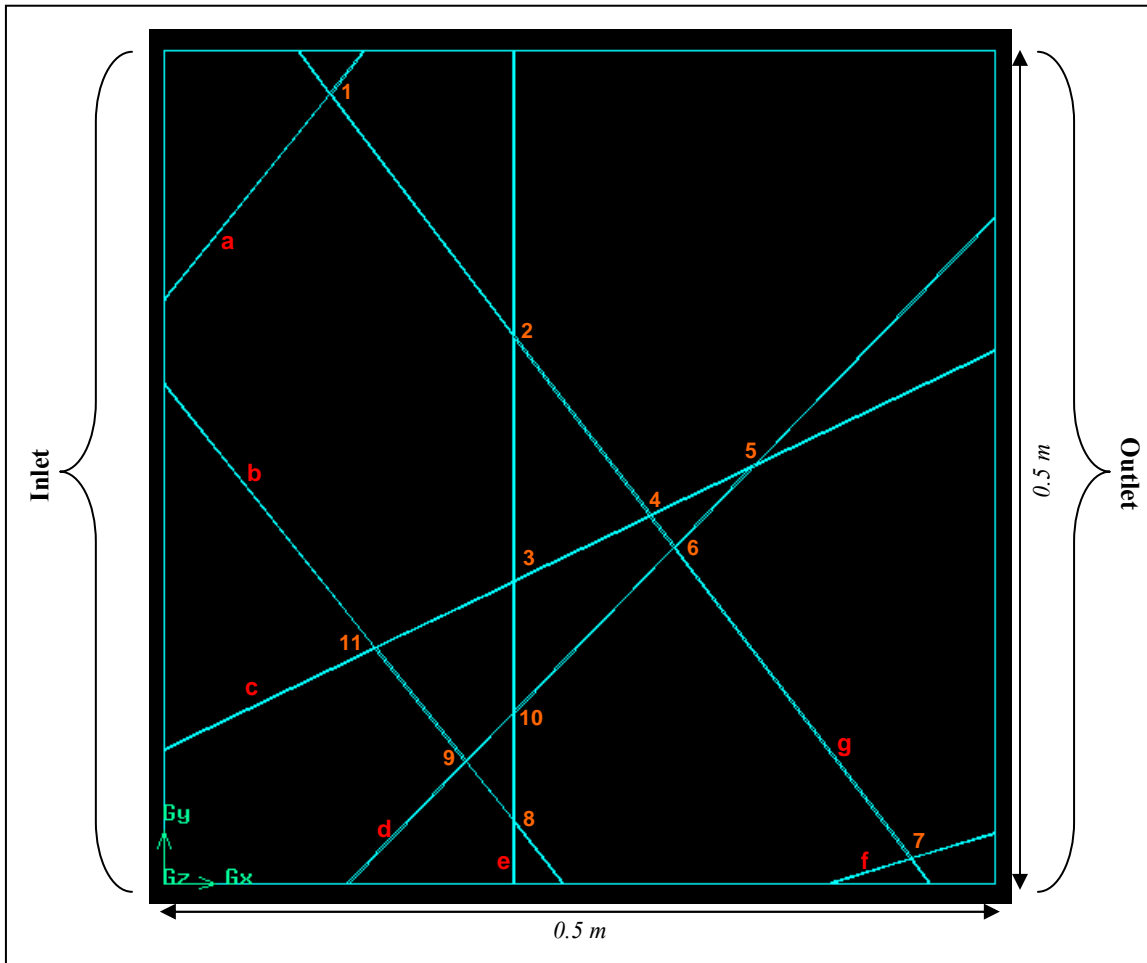
Figure 17: Total seven fractures (numbered a - g), intersecting with each other as shown to form a fracture network. The intersections are also numbered so that they can be referred in some subsequent plots. The true fracture apertures (normal distance between fracture walls) in *mm* are: a – 0.63, b – 0.63, c – 0.9, d – 0.7, e – 1.0, f – 0.96, g – 0.61. For flow simulation purposes, constant static pressures are specified at Inlet and Outlet faces, while the other two opposite faces represent no-flow boundaries. In each individual fracture, fracture walls are impermeable and rigid.
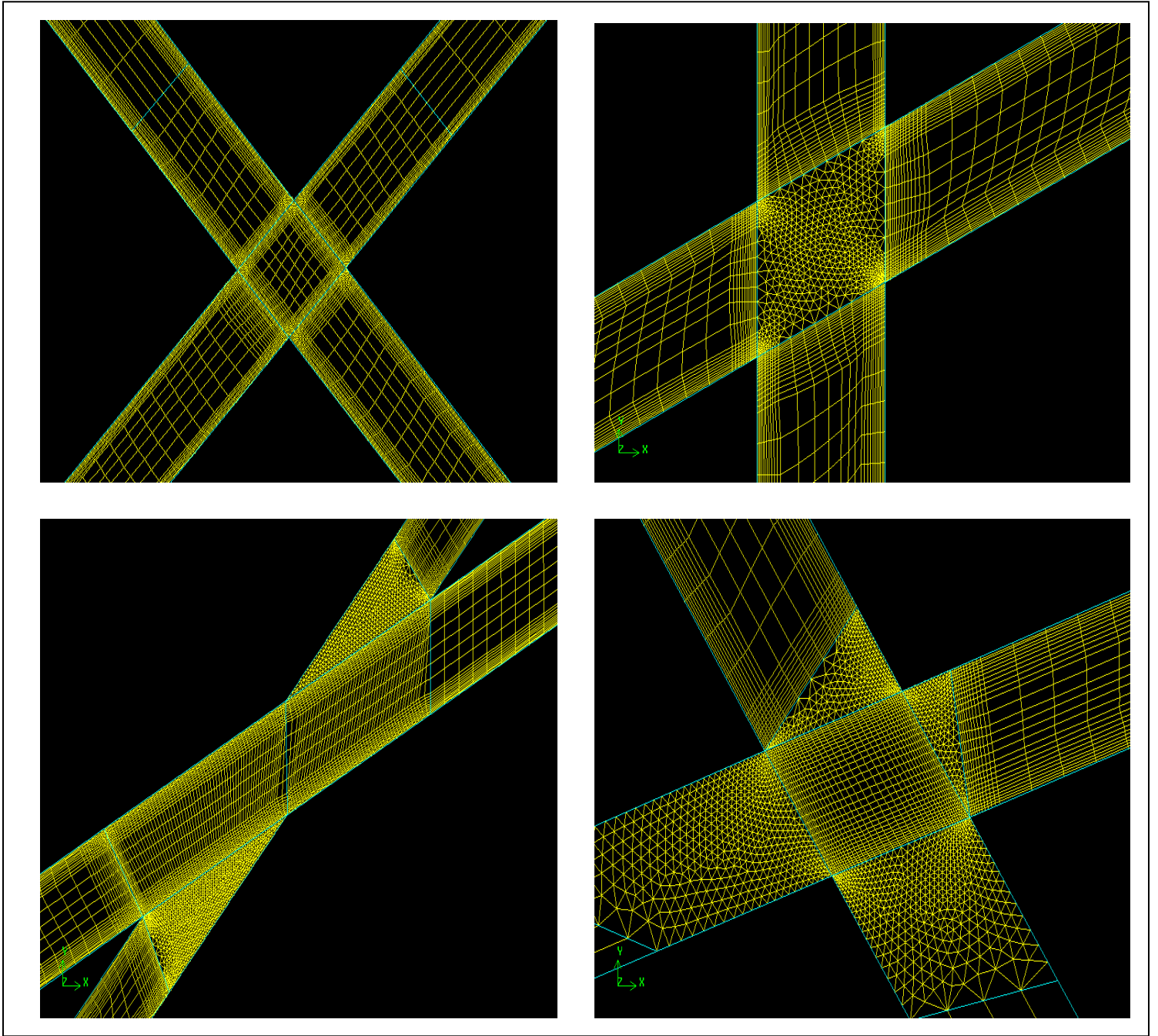
Figure 18: From left to right, top to bottom: mesh used at and around intersection nos. 1, 3, 5 & 7.

Pressure **Velocity magnitude**

Pressure **Velocity magnitude**

Pressure **Velocity magnitude**
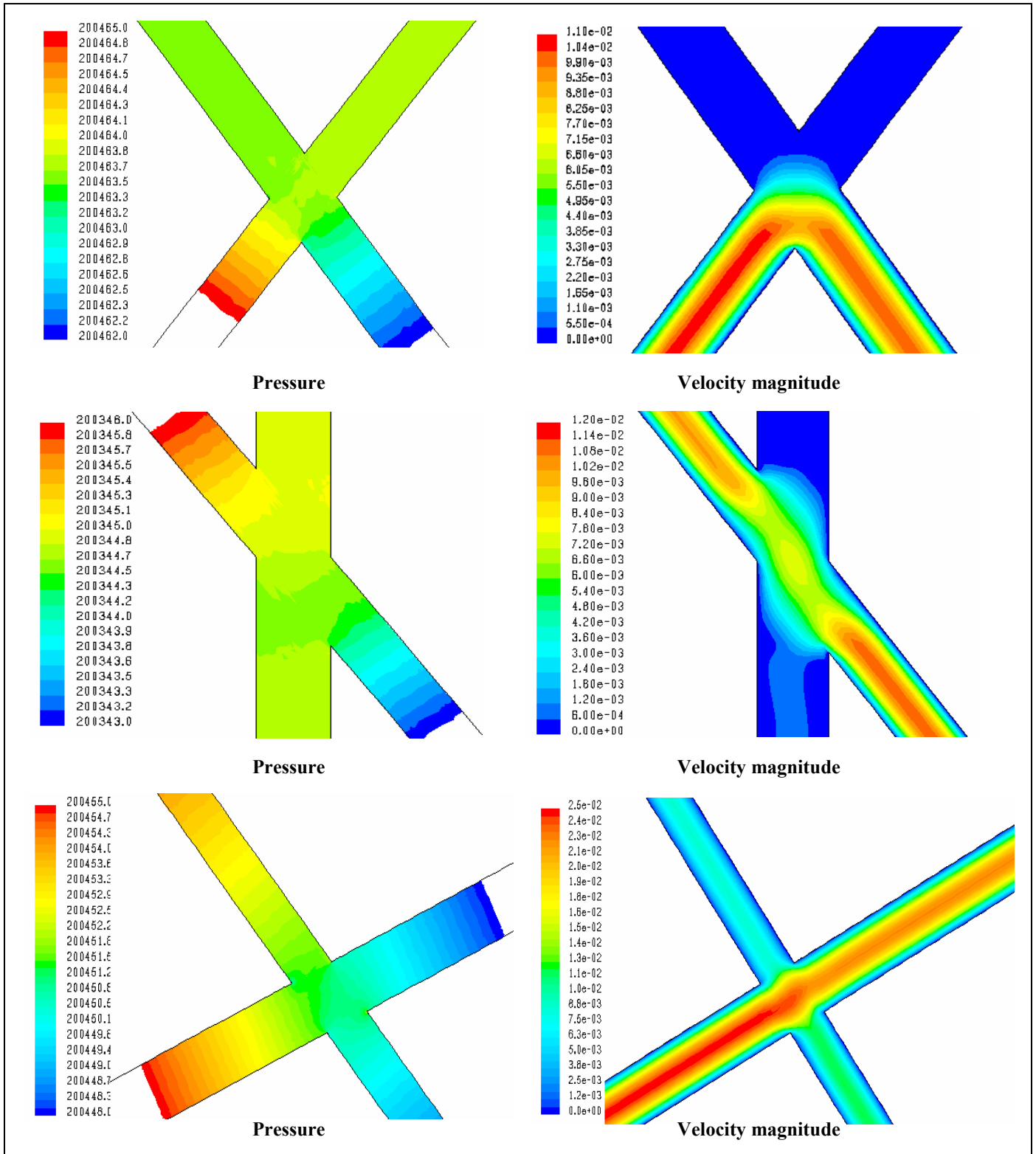
Figure 19: Flow simulation results: from top to bottom – around intersection nos. **1**, **2,** and **11**.
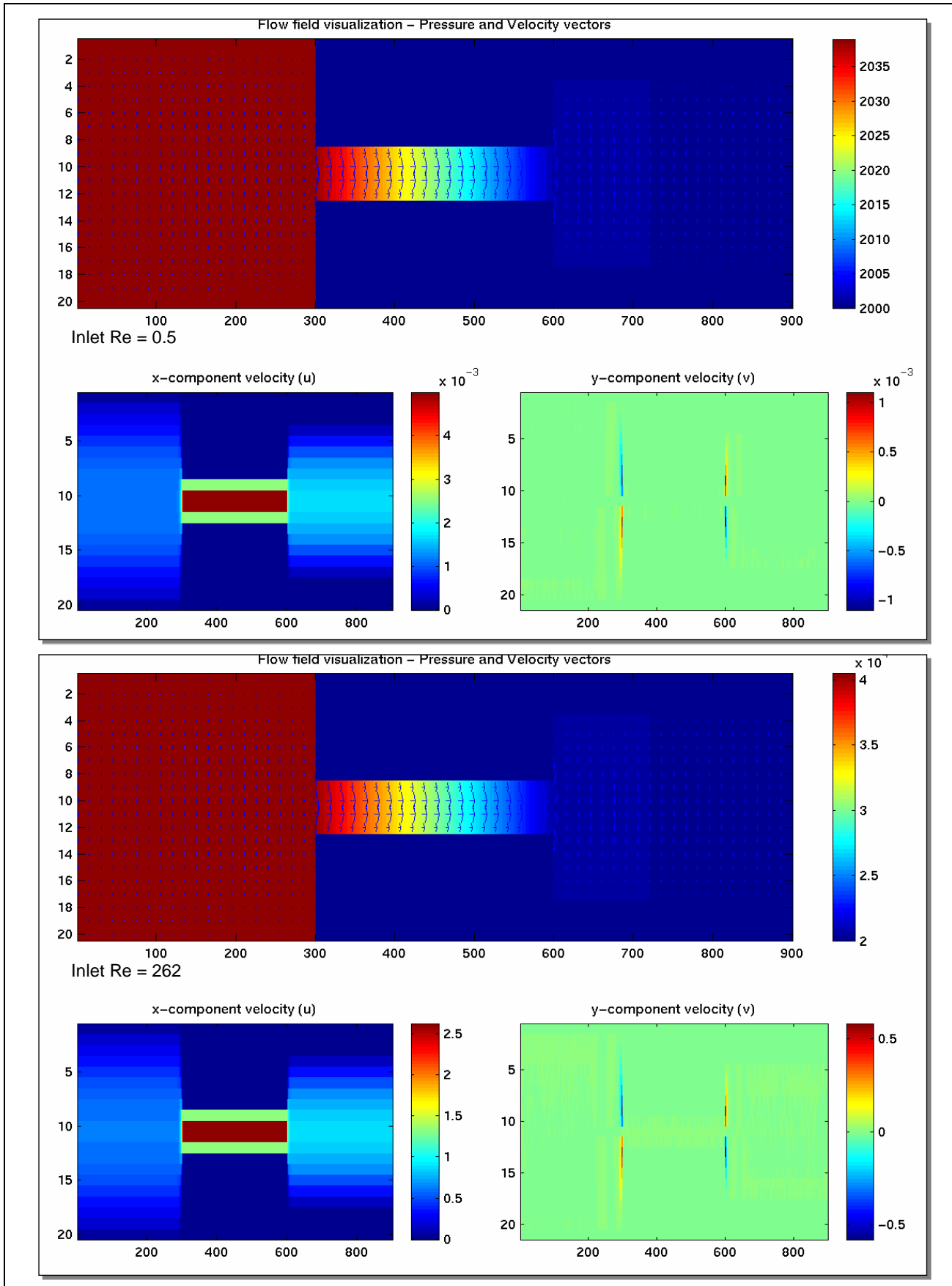
Figure 20: Stokes equation based flow simulation results; top: for ΔP = 39 Pa, bottom: for ΔP = 20466 Pa.
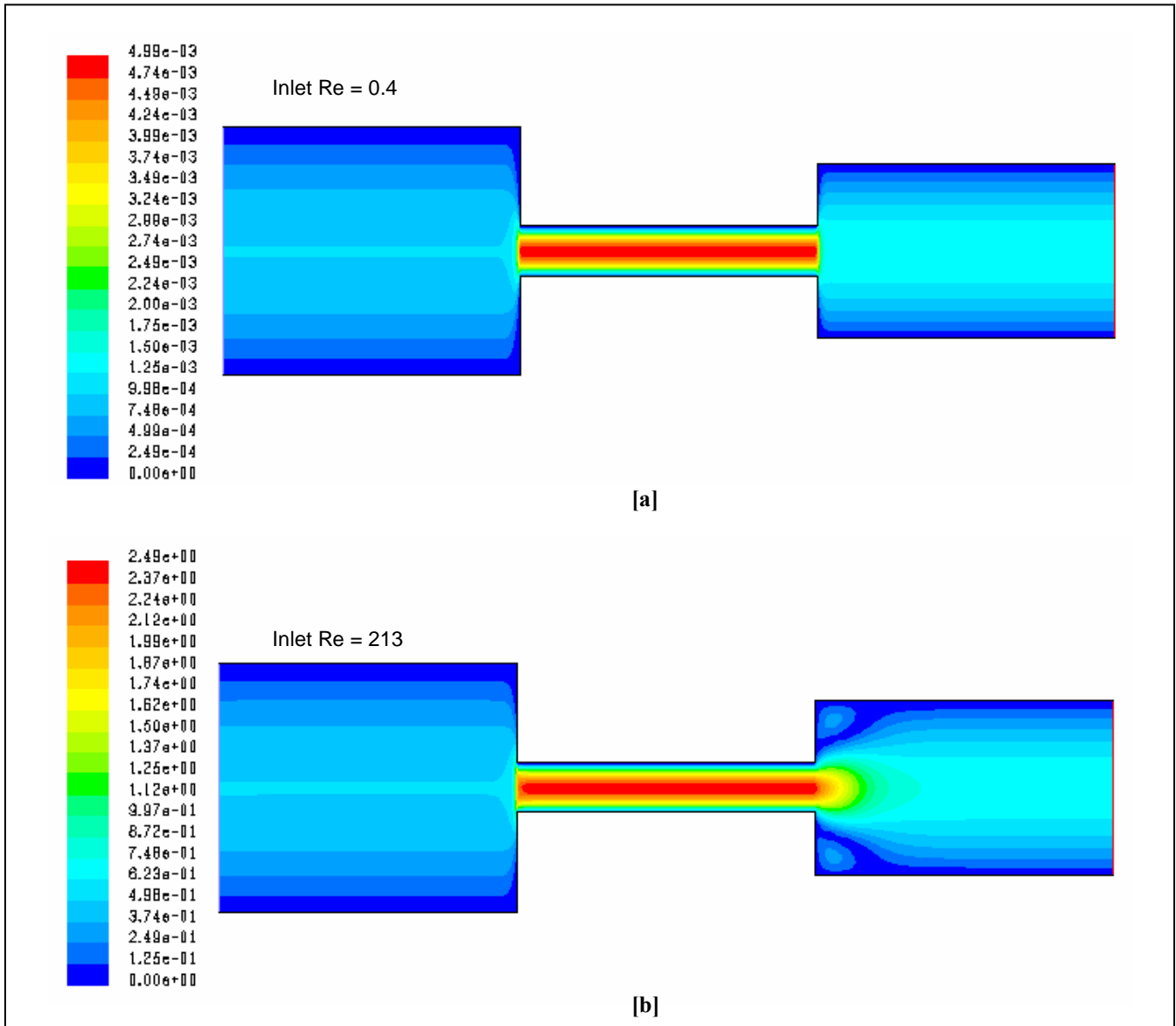
Figure 21: Velocity magnitude contour plots from Navier-Stokes simulation: **[a]** for ΔP = 39 Pa, and **[b]** for ΔP = 20466 Pa.
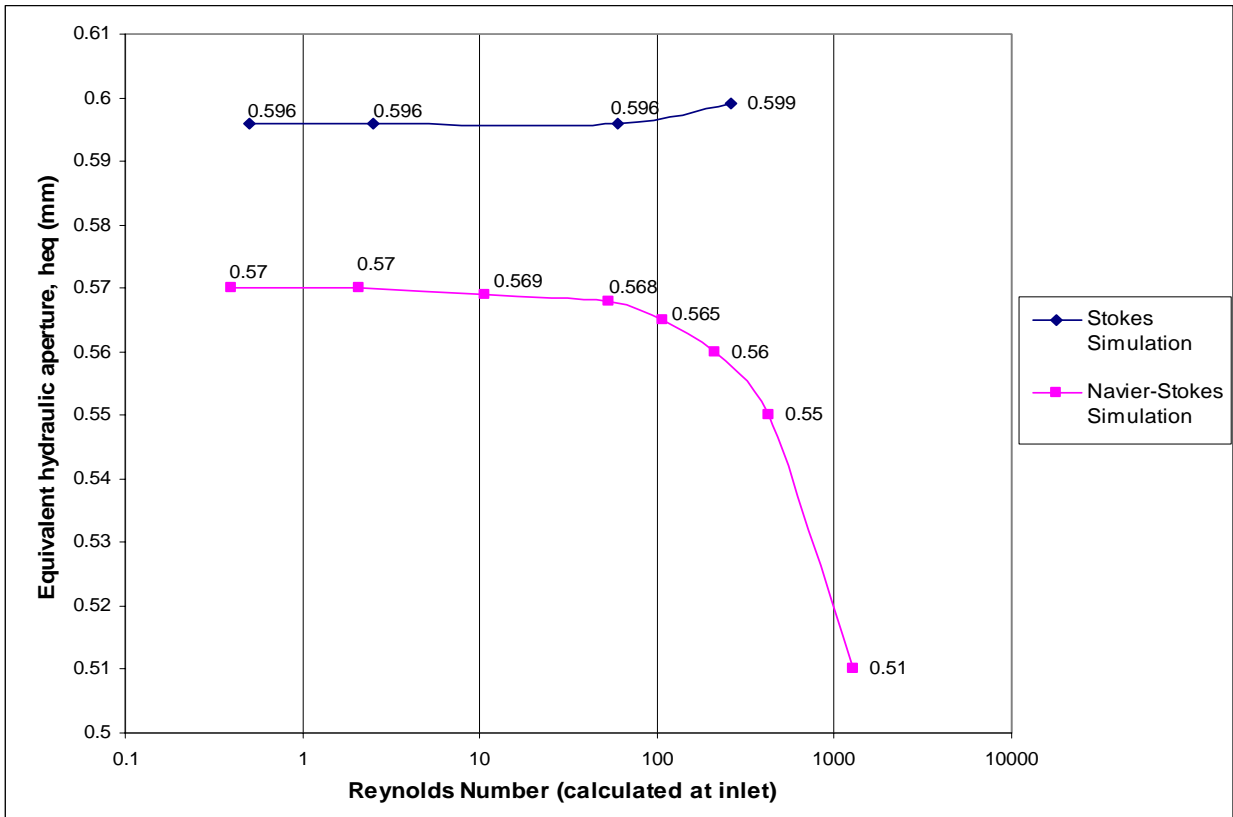
Figure 22: Comparing hydraulic characterization of the series fracture model using two different computational (fluid dynamics) methods.
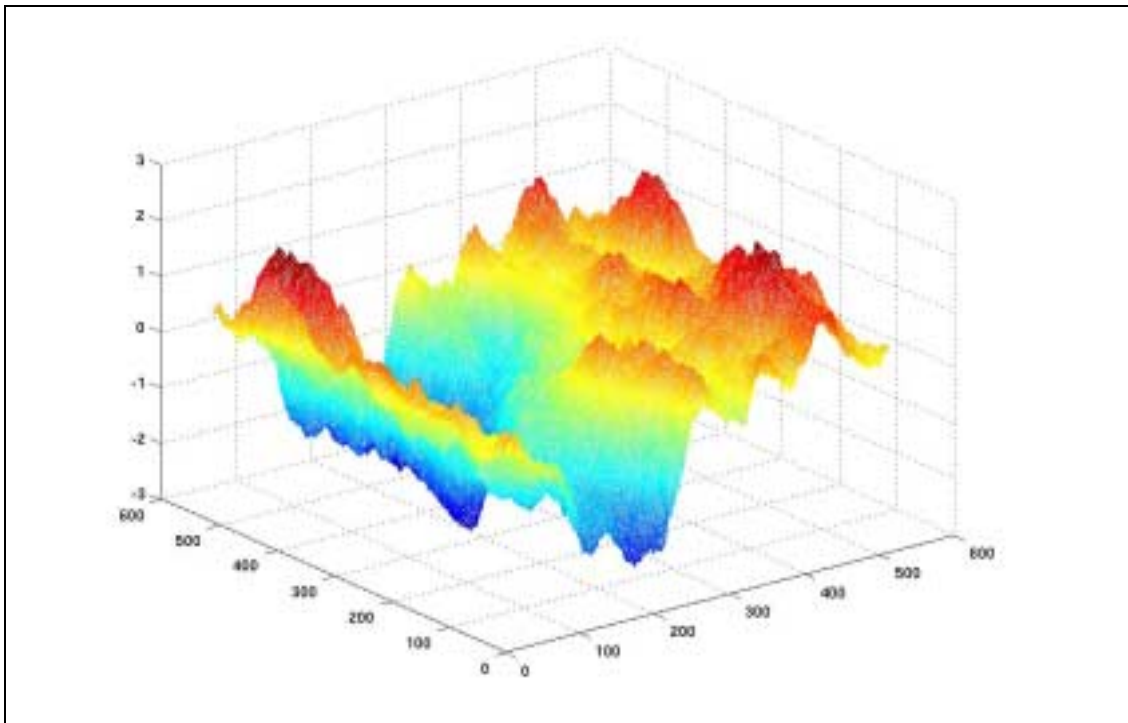
Figure 23: A computer model of a realistic 3D fracture surface.
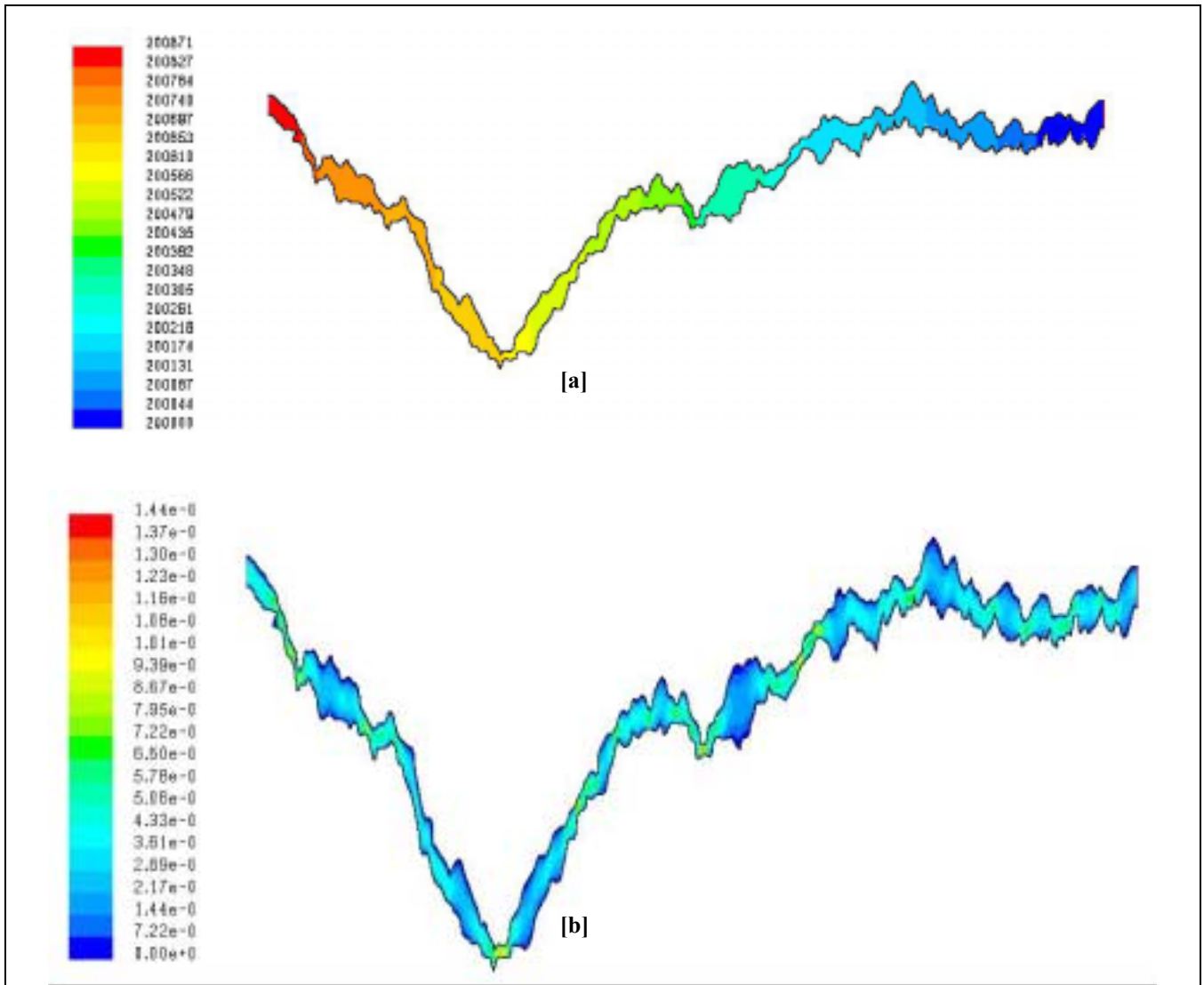
Figure 24: 2D flow simulation in a real fracture: **[a]** Pressure contours, **[b]** Velocity contours.
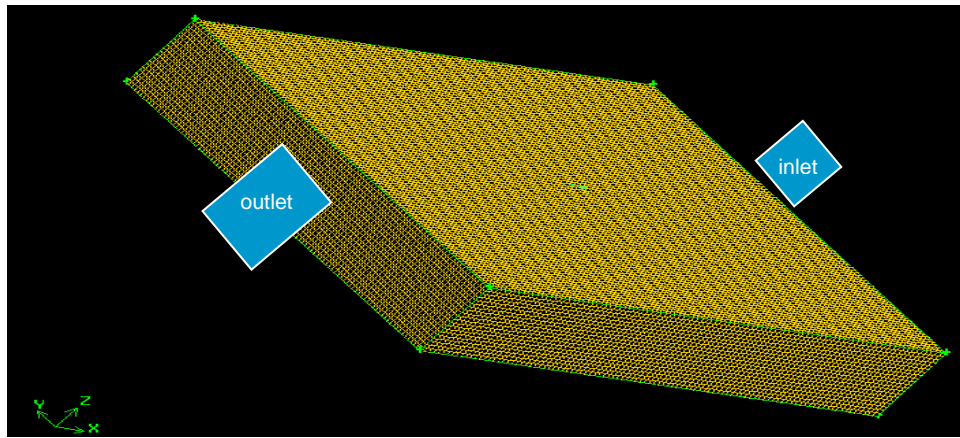
[a]
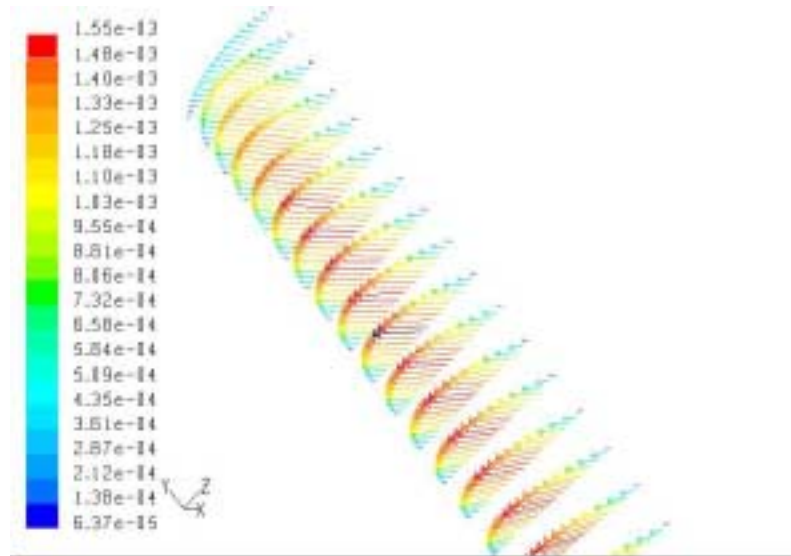
[b]
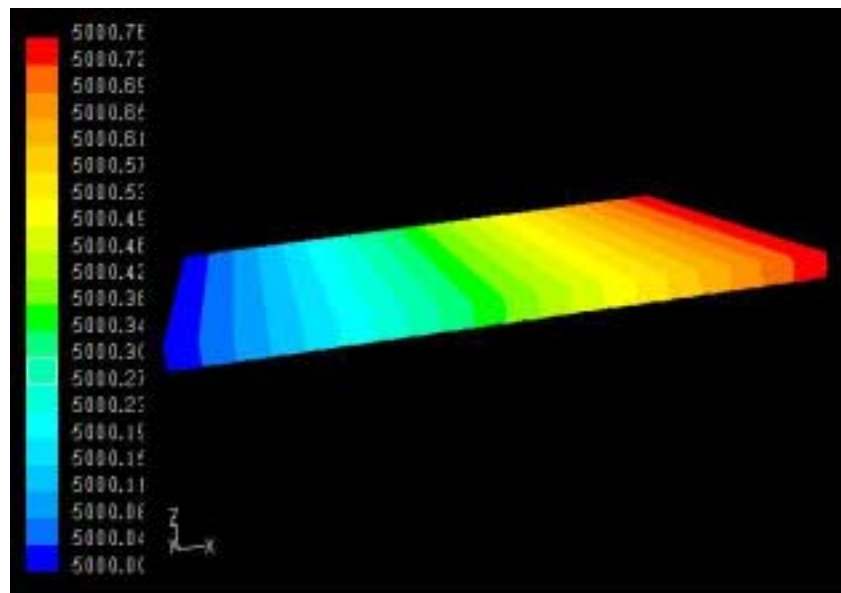
[c]

Figure 25: Flow bounded by parallel plates in 3D (also known as *Poiseulle Flow*): **[a]** Model geometry, with meshes; **[b]** Velocity vectors shown in 3D; **[c]** Pressure distribution (contours) in 3D.
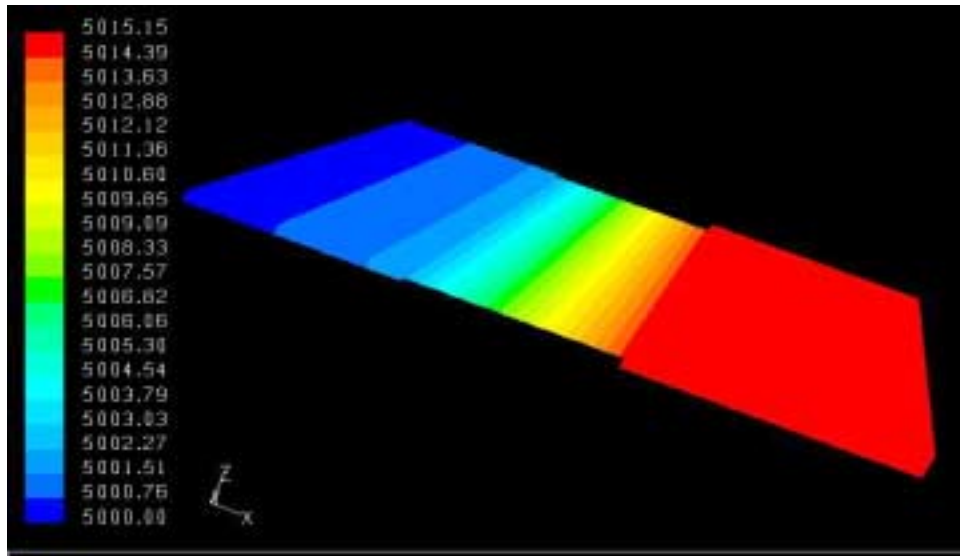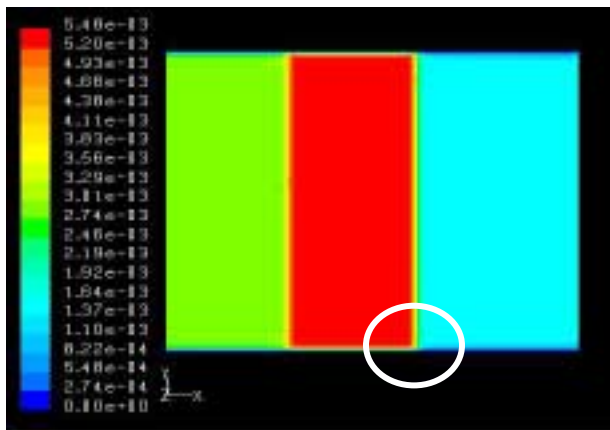
$$u(y,z) = \frac{16a^2}{\mu\pi^3}\left(-\frac{dp}{dx}\right)\sum_{i=1,3,5,\ldots}^{\infty}(-1)^{(i-1)/2}\left[1-\frac{\cosh\left(i\pi z/2a\right)}{\cosh\left(i\pi b/2a\right)}\right]\frac{\cos\left(i\pi y/2a\right)}{i^3}$$

[3]
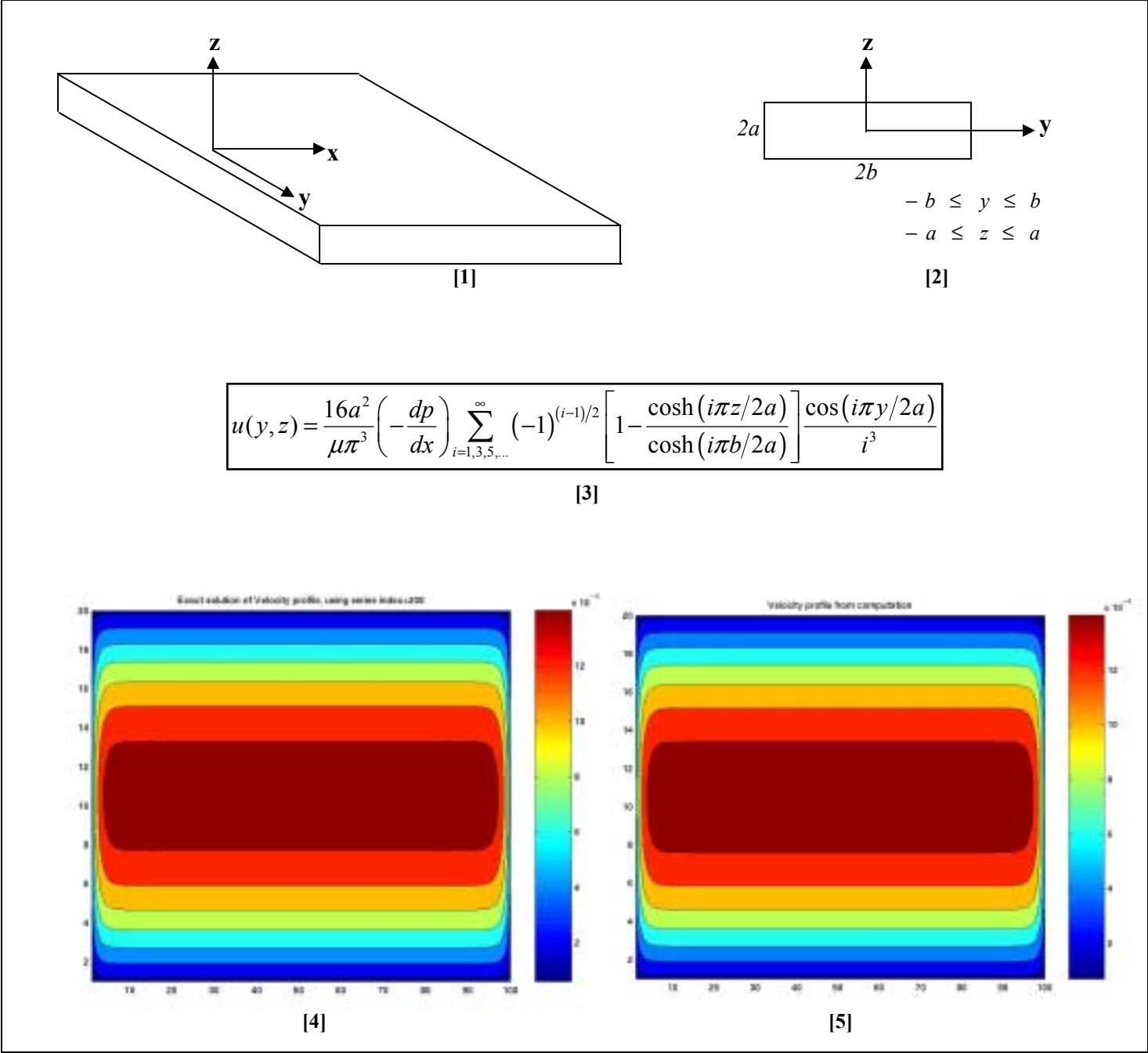
Figure 26: **[1]** 3D brick geometry (*non-circular duct*) and **[2]** constant rectangular cross-section normal to the flow direction. **[3]** Analytical expression for velocity profile (Gursul, 1998). **[4]** Analytical solution for velocity profile using series index *i* up to 200, and **[5]** Velocity profile obtained from flow simulation.
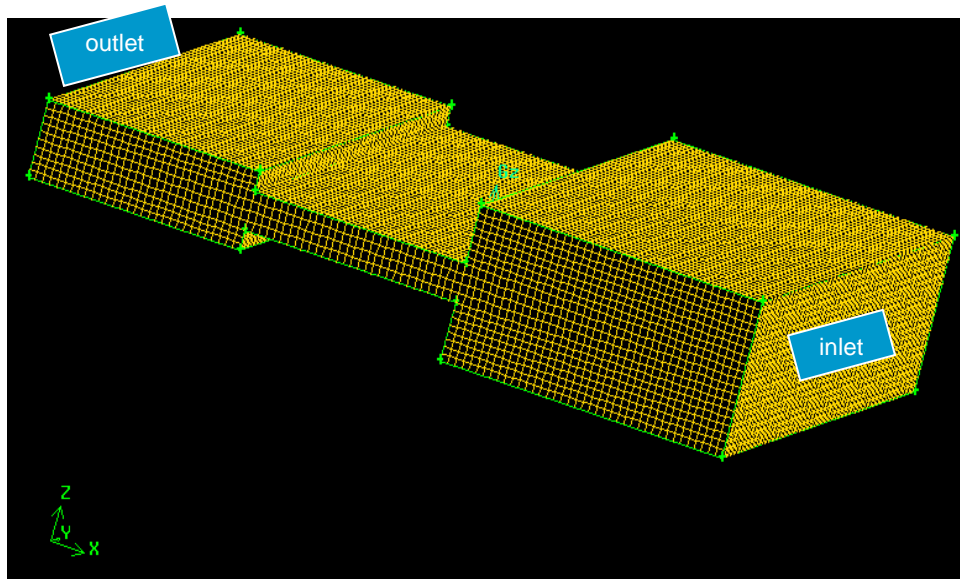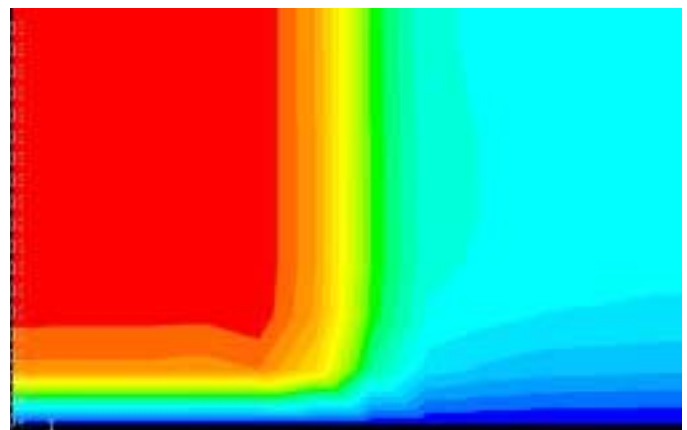
Figure 27: **[a]** 3D flow model (showing meshes as well) with variable aperture. **[b]** Pressure distribution in 3D. **[c]** x-y profile of pressure distribution plotted for a surface z=0 (midway between the two walls), and **[d]** magnified view of the region pointed by white oval on [c] to highlight the non-linearity effect due to aperture change.
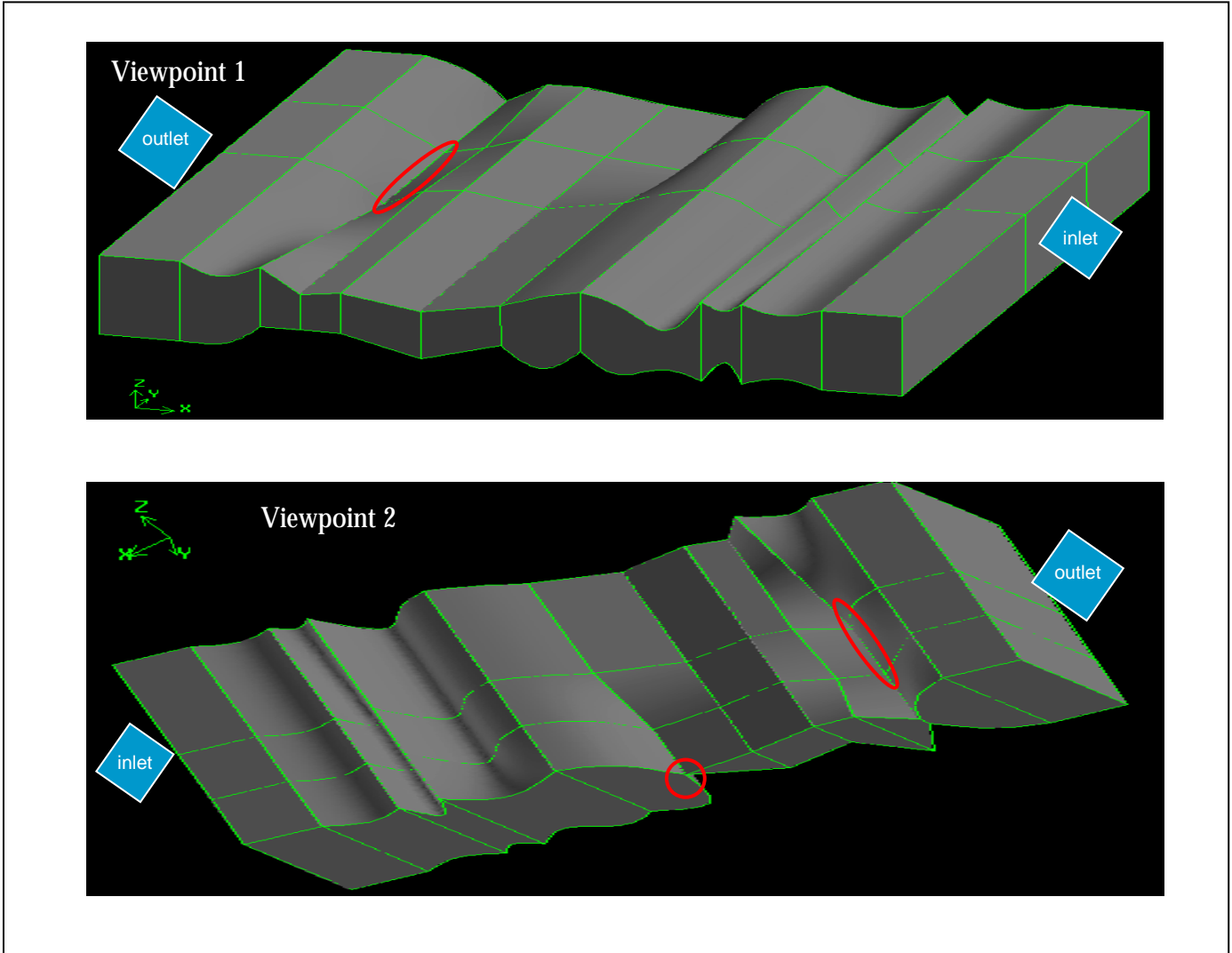
Figure 28: Realistic fracture is 3D having both asperities and asperity contacts. Ovals/circles in red denote asperity contacts present in the model.
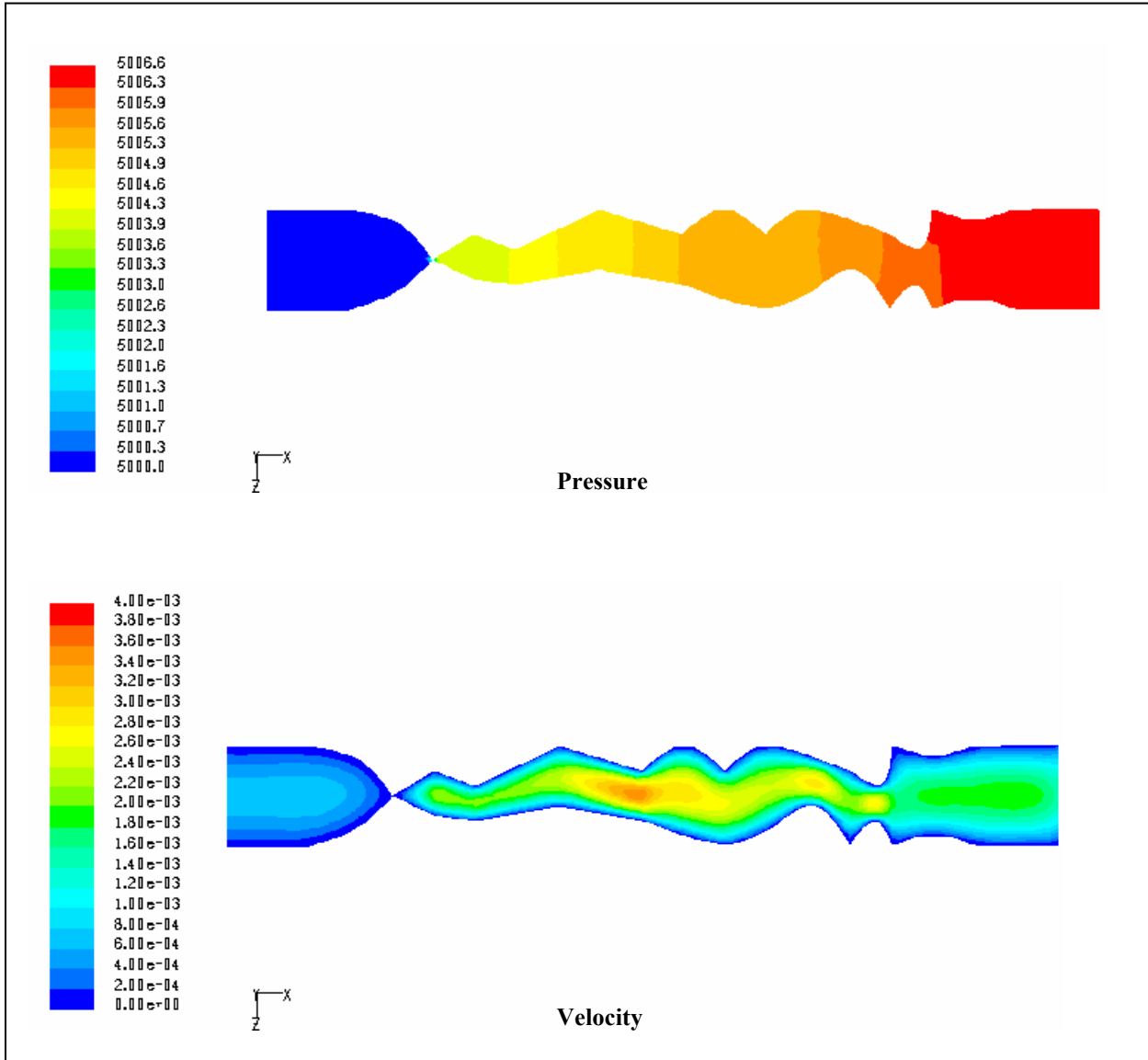
Figure 29: Contour plots along a 2D surface *(y = 0)* drawn from the 3D fracture model of Figure 33.